Negative microfilm 63–478
received from university

WILKINSON, David Todd, 1935–
A PRECISION MEASUREMENT OF THE g–FACTOR OF THE FREE ELECTRON.

University of Michigan, Ph.D., 1962
Physics, general

University Microfilms, Inc., Ann Arbor, Michigan

A PRECISION MEASUREMENT OF THE g-FACTOR OF THE FREE ELECTRON

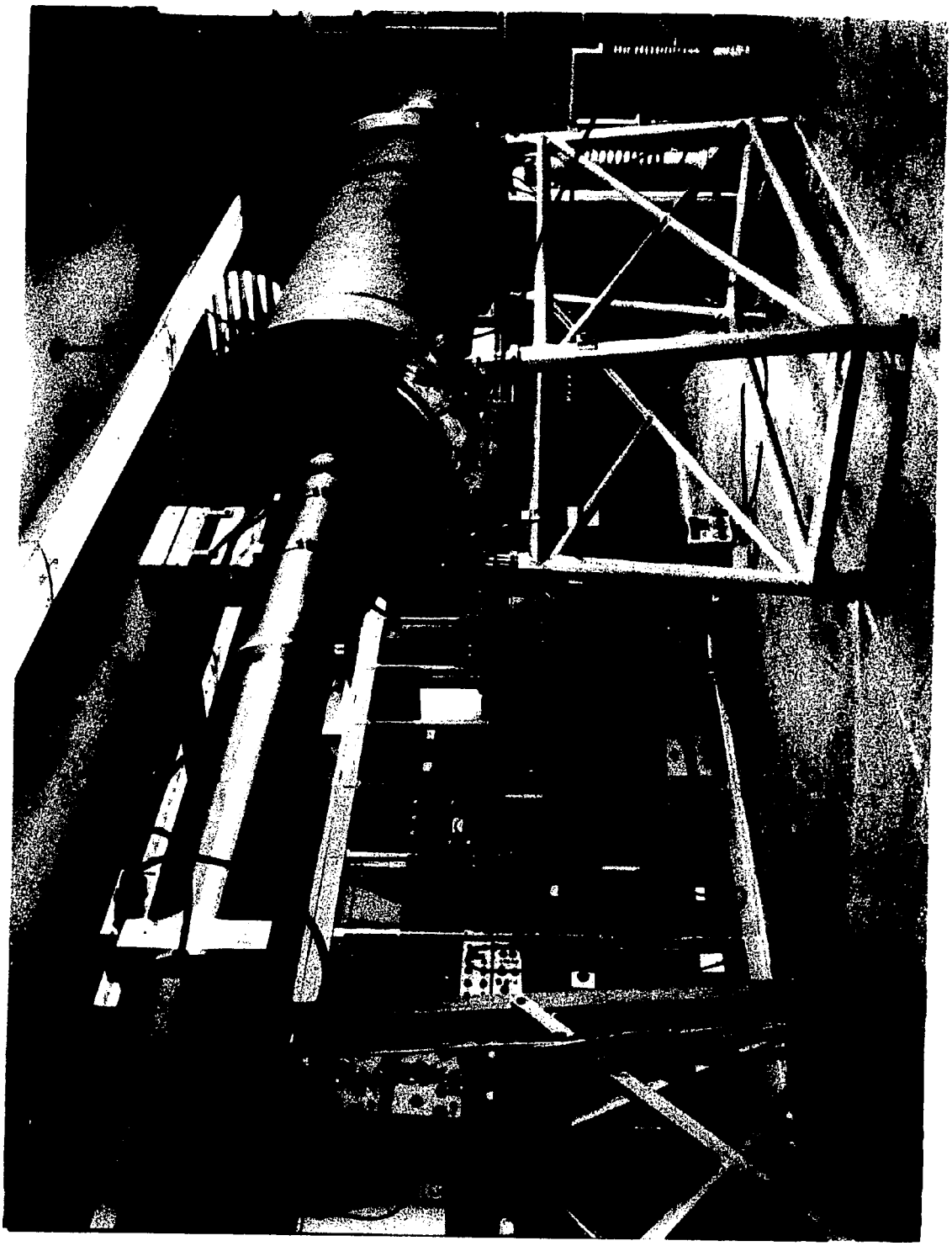
by

David Todd Wilkinson

A dissertation submitted in partial fulfillment
of the requirements for the degree of
Doctor of Philosophy in the
University of Michigan
1962

Doctoral Committee:

Professor H. Richard Crane, Chairman
Associate Professor George W. Ford
Associate Professor Peter A. Franken
Associate Professor Robert R. Lewis
Professor Richard K. Osborn



The Apparatus

DEDICATION

To my parents who devoted many

years to the education of their sons.

PREFACE

The contents of this thesis have been chosen with two types of readers in mind. First, because of the high inherent precision of this experiment, similar techniques will almost surely be employed either to repeat this measurement or as part of other experiments. The reader contemplating such an experiment should find Section 1.2 and Chapter III of particular interest. Detailed descriptions of the apparatus are included with the hope that the designer of future experiments will not repeat our mistakes. Secondly, because of the great importance of this measurement to quantum electrodynamic theory, there should be considerable interest in the methods used to obtain and analyze the data. Section 2.2 and Chapter IV should aid the reader who wishes to check our result in detail. The more casual reader is referred to a forthcoming paper by Professor H. R. Crane and myself which will contain fewer details of the apparatus and analysis.

I would like to express my sincere appreciation to Professor Crane for his guidance and encouragement throughout the course of this work and to the members of my committee for many helpful and enlightening discussions concerning both the experimental and theoretical aspects of this experiment. Also I wish to thank Mr. Harry Westrick whose remarkable mechanical skills contributed greatly to the construction and maintenance of the apparatus. This work was supported generously by the United States Atomic Energy Commission.

TABLE OF CONTENTS

	Page
FRONTISPIECE	ii
DEDICATION	iii
PREFACE	iv
LIST OF FIGURES	vi
I. INTRODUCTION	1
1.1. Historical Sketch	1
1.2. The Present Experiment	6
II. THEORY OF THE EXPERIMENT	10
2.1. Physical Description of the Calculation of "a"	10
2.2. The Difference Frequency in the Trap	13
III. APPARATUS	19
3.1. Design Criteria	19
3.2. Physical Layout	19
3.3. Vacuum System	20
3.4. Magnetic Field	20
3.5. Timing System	24
3.6. Electron Source	25
3.7. Counting System	27
IV. EXPERIMENTAL RESULTS AND ANALYSIS	30
4.1. Measurement and Analysis of the Magnetic Field	30
4.2. Measurement and Analysis of the Difference Frequency	38
4.3. Results, Errors, and Conclusions	43
APPENDICES	
A1. Data for Two Field Mappings	55
A2. Some Quantities Used in Averaging	56
B1. Data for 36 Difference Frequency Runs	57
B2. Computed Maxima and Averages	69
C1. Orbital Precession and the Falloff Index	71
C2. Theoretical Polarization and Asymmetry Amplitude	74
C3. Verification of Equation (4.3)	75
C4. List of Experimental Parameters	78
LIST OF REFERENCES	79

LIST OF FIGURES

Figure		Page
1.	Sketch of g-Factor I.	3
2.	Sketch of g-Factor II	4
3.	The Present Experiment.	7
4.	The Trapping Procedure.	8
5.	Feynman Diagrams	10
6.	First Order Corrections to the Magnetic Moment.	11
7.	Second Order Corrections to the Magnetic Moment	13
8.	Magnetic Field Regulators	22
9.	Timing System	26
10.	Proton Resonance Patterns	31
11.	The Magnetic Field in the Trapping Region	33
12.	Data for the End Points of the First Four Runs.	40
13.	Evaluation of "a"	48
14.	Comparison of Results of g-Factor IIand g-Factor III.	49
15.	Sketch of Beam Cross Section.	71
16.	Counting Rate vs. Trapping Time	72

I. INTRODUCTION

1.1. Historical Sketch

The g-factor of a particle is defined by the relationship

$$\vec{\mu} = \frac{g}{2}\frac{e}{mc}\vec{S}\,, \qquad (1.1)$$

where g, $\vec{\mu}$, $\vec{S}$, and e/m represent the particle's g-factor, intrinsic magnetic moment, intrinsic angular momentum, and charge to mass ratio respectively: cgs. units are used throughout this thesis. Non-relativistic classical mechanics predicts g = 1 for any rotating body with the same charge to mass ratio throughout. However, in 1927, Dirac [1] theoretically predicted an intrinsic magnetic moment for the electron with g = 2. This prediction agreed with an earlier hypothesis set forth by Uhlenbeck and Goudsmit [2] in order to successfully explain the anomalous Zeeman effect.

Dirac theory was very successful in explaining atomic spectra until 1947 when Lamb and Retherford [3], using microwaves, discovered the now famous Lamb shift in hydrogen. Lamb showed experimentally that the $2^2S_{1/2}$ and the $2^2P_{1/2}$ states of hydrogen are not degenerate as predicted by the Dirac equation, but are separated by about 1,000 megacycles. This departure from Dirac theory was very soon shown by Bethe [4] to be the result of radiative corrections to the Dirac theory. Using subtraction techniques, he eliminated the divergences in the old theory and was able to predict a Lamb shift of 1,040 megacycles. This signaled the development of quantum electrodynamics.

In 1948, Schwinger [5] calculated the first order radiative correction to the electron magnetic moment. This so-called anomalous

magnetic moment can be written as a power series in the fine structure constant α. Schwinger showed that for the electron

$$\mu = \mu_0 \left(1 + \frac{\alpha}{2\pi} + \cdots\right) , \tag{1.2}$$

where $\mu_0 = e\hbar/2mc$ is the Bohr magneton. This result is often expressed as a correction to the g-factor of the electron:

$$\frac{g}{2} = 1 + a = 1 + \frac{\alpha}{2\pi} + \cdots , \tag{1.3}$$

where "a" is the anomaly in the g-factor.

The first calculation [6] of the term of second order in α was incorrect. In 1957, Sommerfield[7] reported the value

$$a = \frac{\alpha}{2\pi} - 0.328 \frac{\alpha^2}{\pi^2} + \cdots . \tag{1.4}$$

This result has been checked [8] and is now accepted as correct. Using

$$\alpha = \frac{e^2}{\hbar c} = \frac{1}{137.0391 \pm 0.0006} , \tag{1.5}$$

the numerical value of "a" is

$$a = 0.001\ 159\ 61 \pm 0.000\ 000\ 01 . \tag{1.6}$$

The first quantitative measurement of "a" was made by Kusch and Foley[9]. Using atomic beam measurements of Zeeman splitting in Ga, In, and Na, they obtained

$$a = 0.001\ 19 \pm 0.000\ 05 . \tag{1.7}$$

More accurate results have been reported by Franken and Liebes [10]:

$$a = 0.001\ 168 \pm 0.000\ 009 , \tag{1.8}$$

and by Hardy and Purcell [11]:

$$a = 0.001\ 156\ 1 \pm 0.000\ 001\ 5 \quad . \tag{1.9}$$

These values were obtained by measuring the magnetic moment of protons in oil in units of the Bohr magneton, $\mu_p(\text{oil})/\mu_o$, and multiplying by the accurately measured value [12-15] of $\mu_e/\mu_p(\text{oil})$. The uncertainties quoted are limits of error and arise from magnetic field inhomogeneities, relativistic effects, and resonance line asymmetries.

A more direct measurement was proposed by Crane in 1950 and carried out by Crane, Pidd, and Louisell [16]. The experiment, shown in Figure 1, is simply a Mott double scattering experiment with a magnetic field between the two scattering foils. The electron beam is partially polarized by the first foil in a direction perpendicular to the scattering plane. The polarization direction then precesses about the magnetic field with the Larmor frequency

$$\vec{\omega}_L = \frac{ge}{2mc}\vec{B} \quad . \tag{1.10}$$

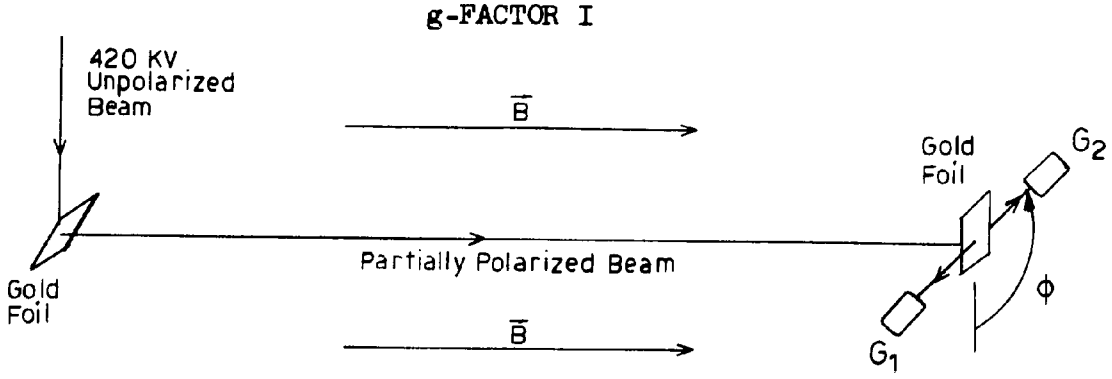


Figure 1.

The direction of polarization at the second foil is found by measuring the intensity asymmetry in a plane normal to the incident beam.

The asymmetry is maximum in a direction perpendicular to the polarization. By measuring the magnetic field, the time spent in the field, and the total angle of rotation of the polarization between foils, the value $g = 2.00 \pm 0.01$ was obtained. The accuracy of the result was limited by the small number of rotations (about 5) of the polarization. The experiment, however, demonstrated that the g-factor of the free electron could be measured. There was some doubt about this at the time [17].

It was recognized that the way to improve g-Factor I was to increase the time which the electrons spend in the magnetic field and, thereby, increase the number of rotations of the polarization between scatterings. This can be accomplished by rearranging the first scattering in such a way that a pulse of electrons is scattered into a direction nearly perpendicular to the magnetic field. The resulting orbit is a helix of small pitch spiralling down the magnetic field as shown in Figure 2. The beam is then trapped by reducing the axial momentum of the electrons and leaving them in a magnetic bottle. Electrons are ejected from the trap at a measured time after injection and scattered from a second gold foil. The intensity

g-FACTOR II

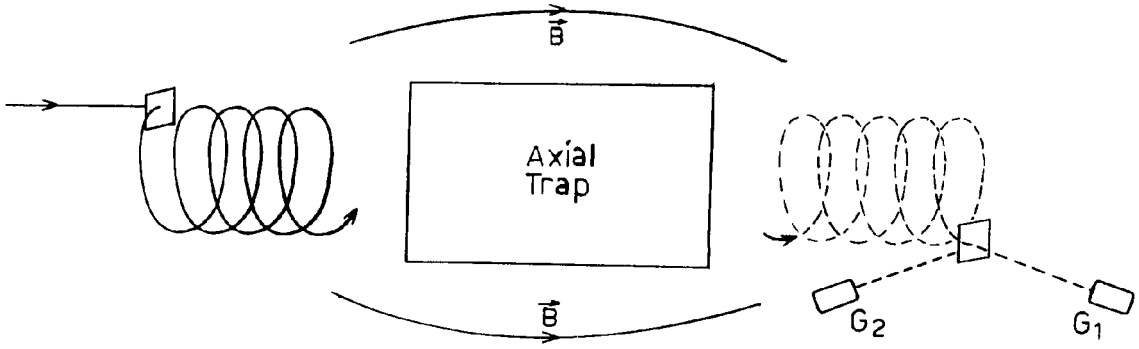


Figure 2.

asymmetry $(G_1 - G_2)$ as a function of trapping time is then a cosine curve whose frequency is the difference between the spin precession frequency (as measured in the laboratory system) and the orbital (cyclotron) frequency.

This difference frequency was calculated by Mendlowitz and Case [18] for orbits perpendicular to a homogeneous magnetic field. They found

$$\omega_D = \omega_s - \omega_c = \omega_o a \quad , \tag{1.11}$$

where

ω_s = spin precession frequency (in lab. system),

ω_c = cyclotron frequency = $-eB/\gamma mc$; $\gamma = (1 - v^2/c^2)^{-1/2}$,

ω_o = zero energy cyclotron frequency = $- eB/mc$.

Therefore, "a" is measured <u>directly</u> by measuring ω_D and B. The fact that ω_s and ω_c differ only because of the radiative corrections makes this a very sensitive measurement of the g-factor.

This experiment (hereafter referred to as g-Factor II) was done by Crane, Pidd and Schupp [19] with the following result:

$$a = 0.001\ 160\ 9 \pm 0.000\ 002\ 4 = \frac{\alpha}{2\pi} - (0.1 \pm 0.4)\frac{\alpha^2}{\pi^2} \quad , \tag{1.12}$$

in good agreement with theory but falling just short of checking the α^2 term in (1.4).

The principal sources of error were: (1) uncertainty in the average magnetic field which the electron experiences while in the trap, (2) statistical errors in measuring ω_D, (3) unmeasured radial electric fields which produce energy dependent shifts according to the equation

$$\frac{\omega_D}{\omega_o} = a + \frac{E}{cB}\frac{\beta^2 - 1}{\beta} \quad , \tag{1.13}$$

where E is the average radial electric field and $\beta = v/c$.

1.2. The Present Experiment

The motivation for seeking a more precise measurement of "a" is clear. A factor of 10 improvement in the accuracy of g-Factor II gives the first check on the α^2 radiative correction term in (1.4). The contribution of this term to the Lamb shift [20] is about 0.1 megacycles, whereas, the ultimate experimental accuracy seems to be $\pm$ 0.1 megacycles [21]. In addition the present experiment is a very sensitive test for a possible electric dipole moment for electrons.

Figure 3 shows a cut-away sketch of the present experiment. A 0.2 microsecond pulse of electrons is emitted from the gun and scattered from a gold foil polarizing target. Only electrons which are scattered into angles which give helical orbits of small pitch are allowed to enter the trapping region. Since the scattering angle is nearly 90° the scattered beam is about 25% polarized [21] in a direction normal to the scattering plane.

The beam is trapped as follows. The magnetic field in the trapping region is bottle shaped (see Figure 3) and thus creates an axial energy well for electrons spiraling down the field. Since magnetic forces are conservative, the beam must be injected into and ejected from the well. This is accomplished by applying pulsed electric fields across the gap in the trapping cylinders at the center of the magnetic well. The trapping procedure may be visualized with the aid of Figure 4. At the time of injection a negative voltage is applied to the right hand cylinder and the beam, spiralling in from the left, loses axial momentum as it crosses the gap. This is illustrated in Figure 4(a): the positions of

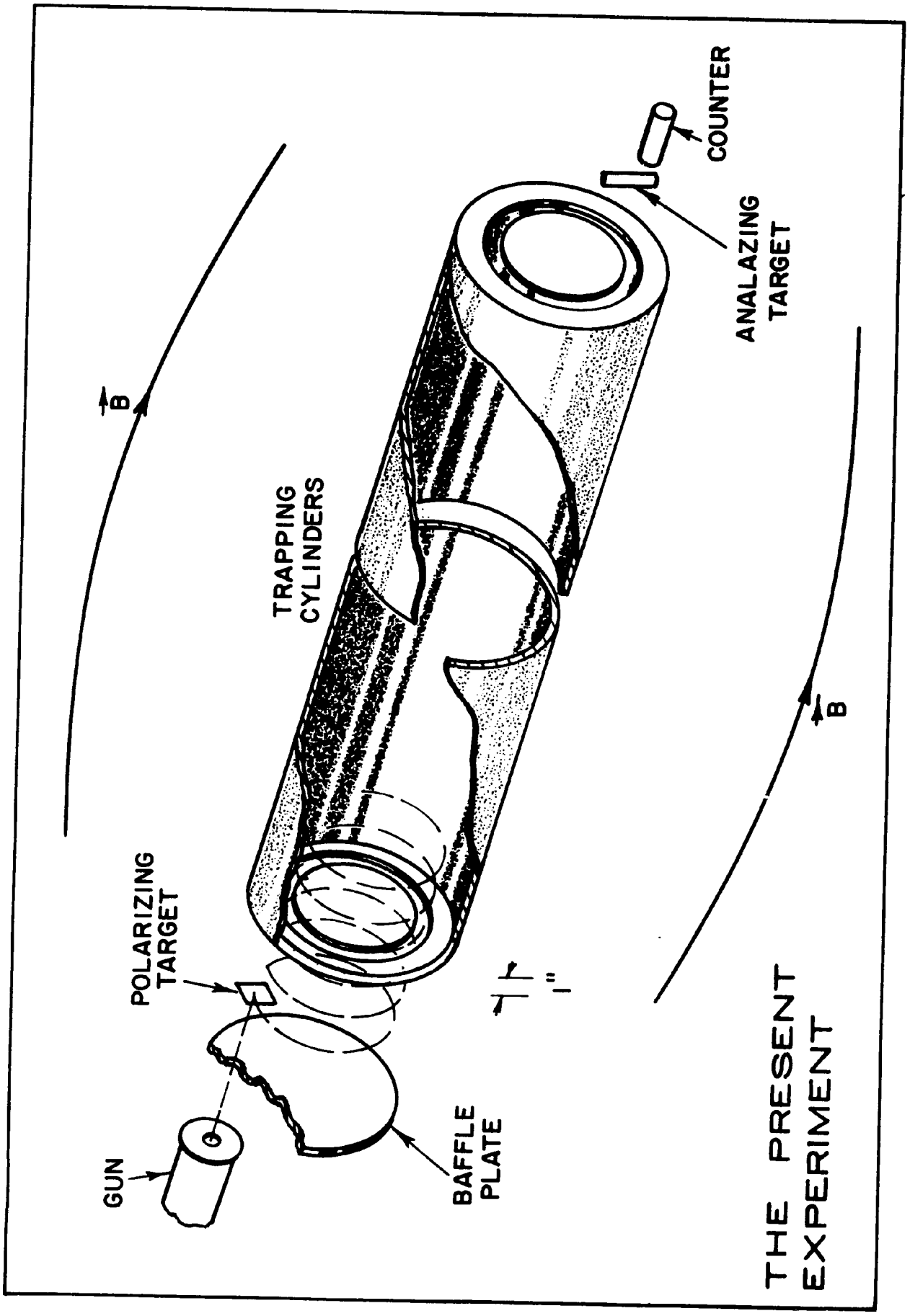

THE PRESENT EXPERIMENT
B
B
GUN
POLARIZING TARGET
BAFFLE PLATE
TRAPPING CYLINDERS
ANALAZING TARGET
COUNTER

Figure 3

THE TRAPPING PROCEDURE

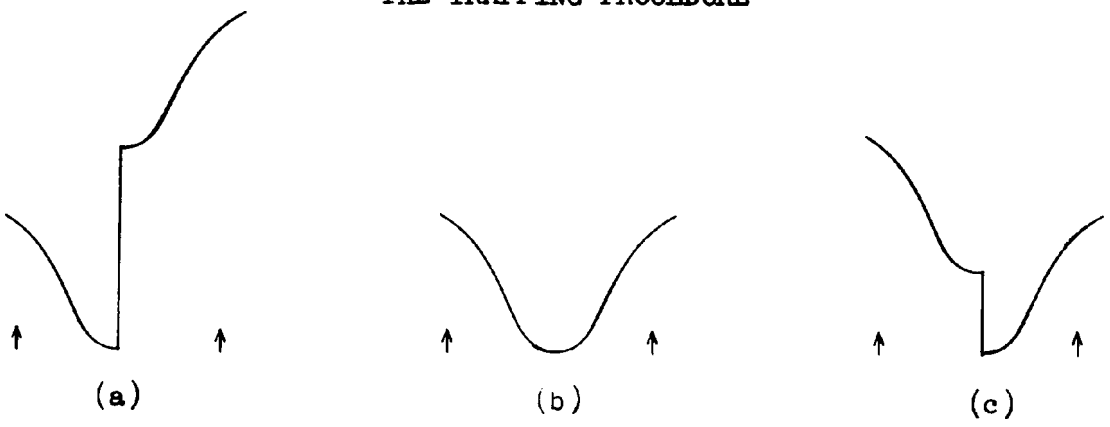


Figure 4.

the scattering foils are indicated by arrows. Some electrons of the beam will get across the gap but be turned around by the magnetic forces in the right-hand side of the well. Before these electrons get back to the gap, the electric field is removed and the electrons do not regain the axial momentum which they lost upon first crossing the gap. They are now trapped in the well of Figure 4(b). To eject electrons from the trap a negative voltage is applied to the left hand cylinder, causing electrons which are inside it to gain axial momentum when they again cross the gap. Thus, they leave the trap to the right. This situation is shown in Figure 4(c). Notice that the electrons which were in the right hand cylinder at the time of ejection remain in the trap, hence, the ejection process is only 50% efficient.

The time which electrons spend in the magnetic field (trapping time) is controlled by the time between the injection and ejection pulses. The polarization of the beam at ejection is measured by the intensity asymmetry from the second scattering foil. As in g-Factor II the asymmetry is measured as a function of trapping time and a cosine curve is traced out whose frequency is given by (1.11). Again, "a" is measured by measuring ω_D and B as accurately as possible.

Several important refinements of g-Factor II have contributed to the increased accuracy of the present experiment. (1) The magnetic field is measured and regulated by proton resonance devices and the magnetic well depth has been reduced by a factor of 5. These improvements permit specification of the average magnetic field to $\pm$ 0.006%, a factor of 20 improvement over g-Factor II. (2) The trapping region has been redesigned to minimize stray electric fields due to surface charging. The trapped electrons are surrounded by cleaned and baked copper surfaces. There is no material inside the beam radius, therefore, all electric fields due to surface charging average to zero except those which pierce the ends of the cylindrical trapped beam. Electric fields from the beam itself and from ions circulating in the trap must be considered. (3) Only one counter is used to detect the asymmetry from the analyzing target. A single counter and slit system has two great advantages. (a) Instrumental asymmetries due to misalignment of two slit systems, and scattering angle asymmetries due to the pitch of the beam are both eliminated. (b) The single counter, on the opposite side of the analyzing target from the trapping region, can be placed at the scattering angle giving maximum asymmetry without getting into the beam path. The mechanics of the single counter scheme are discussed in Section 3.7. (4) High vacuum techniques have been employed, contributing to a factor of 10 increase in beam lifetime. (5) Zero trapping time is not used in the measurement of ω_D, thus avoiding several systematic and random errors discussed in Section 4.2.

II. THEORY OF THE EXPERIMENT

2.1. Physical Description of the Calculation of "a"

This section is included only for the reader who is not familiar with quantum electrodynamics and wishes to get a feeling for the causes of the anomaly in the electron g-factor. It is not a theoretical calculation of "a." Feynman diagrams, which can be used as a starting point for the calculations are discussed and the results are given. The detailed calculation can be found in most introductory texts [23,24].

The quantization of the classical electromagnetic fields has led to their interpretation as clouds of particle-like photons. Thus, electromagnetic interactions can be described as the interactions of photons and charged particles. These interactions are represented schematically by Feynman diagrams which can be converted directly into equations by following well-established rules. Figure 5(a) shows a "bare" electron (solid line) being scattered from an external field (broken line with x): this might be Coulomb scattering, bending in a magnetic field, etc.

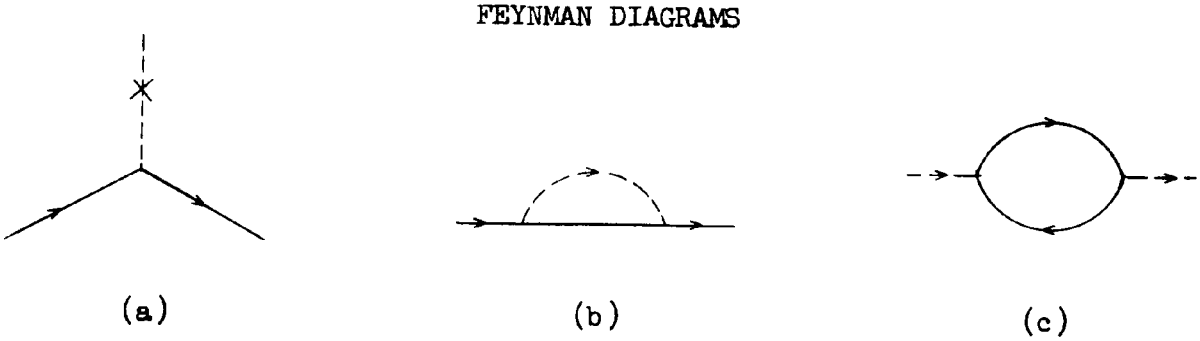


Figure 5.

The electron is "bare" because the photon cloud which surrounds a real electron has been ignored. Figure 5(b) shows the partial conversion of

a bare electron into a real electron by allowing it to interact with a photon (broken line with arrow) from its photon cloud. This is called the electron self-energy diagram and if used in Figure 5(a) in place of the bare electron lines it contributes radiative connections of order α to the bare electron result. Figure 5(c) represents a radiative correction to the photon line due to the possibility of creation and subsequent annihilation of electron-positron pairs. This so-called photon self-energy or vacuum polarization will also give rise to radiative corrections of order α in the processes described by Figure 5(a).

In order to identify the magnetic dipole moment of the electron its interaction with a homogeneous magnetic field is studied. Ignoring radiative corrections, Figure 5(a) is used to calculate the results of such an interaction. The magnetic moment without radiative corrections is found to be the same as that predicted by Dirac theory: only now m and e must be thought of as the mass and charge of the bare electron. In order to calculate the first order radiative corrections to the electron magnetic moment, Figure 5(a) is modified to allow for electron self-energy and vacuum polarization. Figures 6(a) and 6(b) show the electron self-energy modifications to the basic diagram and Figure 6(c) shows the effect of vacuum polarization. The only other contributing diagram is 6(d) which is called the vertex modification. Here the electron interacts with its own field while it is being scattered by the external field. The results of these modifications are summarized on the following page.

α RADIATIVE CORRECTIONS

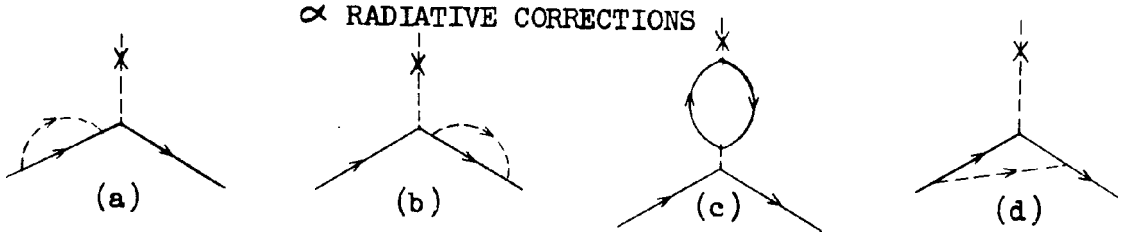


Figure 6.

Electron self-energy corrections, Figures 6(a) and 6(b), contribute:

(i) renormalization of the mass by adding a correction term which partially converts the bare mass into the observed mass. The correction term is logarithmically divergent for large photon momenta,

(ii) renormalization of the charge of the bare electron by adding a correction term which is also logarithmically divergent.

The vacuum polarization correction, Figure 6(c), contributes:

(iii) another charge renormalization,

(iv) finite observable radiative correction of order α.

The vertex modification, Figure 6(d), contributes:

(v) a charge renormalization which just cancels (ii) above,

(vi) finite observable radiative correction of order α.

The effects of mass and charge renormalization are of course not observable because they only convert the theoretical bare electron into an observable electron. Although two of the effects are observable, it turns out that only the vertex modification contributes to the radiative correction of the electron magnetic moment. The well-known result of this calculation is given by (1.2).

The radiative corrections to second order in α follow from Feynman diagrams which modify Figure 5(a) and have five vertices. These diagrams are shown in Figure 7 and their interpretations are similar to those of Figure 6. The figures involving modifications of only external lines have been omitted because, as before, they do not contribute observable corrections. The degree of complexity of this calculation is indicated by the fact that the value $2.973\,\alpha^2/\pi^2$ was reported in 1950 [6] and was

used extensively until 1957 when the calculation was repeated [7,8] giving $0.328\,\alpha^2/\pi^2$.

α^2 RADIATIVE CORRECTIONS

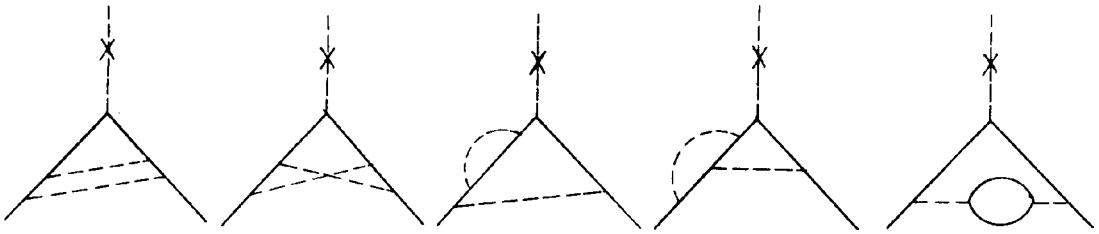


Figure 7.

The divergent results of the mass and charge renormalization terms were a major difficulty in the development of quantum electrodynamics. The perturbation-type methods used in expanding in powers of α certainly are not valid mathematically when individual terms diverge. Apparently, the only justification for interpreting these divergent terms as corrections to the bare charge and mass has been the remarkable success of the theory in predicting the Lamb shift and the anomalous magnetic moment of the electron.

2.2. The Difference Frequency in the Trap

Equation (1.11) gives the difference frequency (ω_D) for electrons moving perpendicular to a homogeneous magnetic field. In order to do a precision experiment, the difference frequency must be found taking into account; (1) the slight inhomogeneity of the magnetic field due to its bottle shape, (2) the finite pitch of the trapped beam, (3) possible electric fields in the trapping region, and (4) a possible electric dipole moment for electrons. The calculation can be done using a classical model and relativistic classical mechanics. The result is then identified with

the expectation value of the quantum mechanical difference frequency. That is

$$\omega_s = \left\langle \frac{2\pi}{\tau_s} \right\rangle , \tag{2.1}$$

where τ_s is the time for a spin flip. The justification for this identification is furnished by an extension of Ehrenfest's theorem.

Ford and Hirt have shown that for a classical particle with

$$\text{magnetic dipole moment} = \frac{ge}{2mc} \vec{S} , \tag{2.2}$$

and

$$\text{electric dipole moment} = \frac{fe}{2mc} \vec{S} , \tag{2.3}$$

the spin precession frequency as viewed from the laboratory frame is

$$\vec{\omega}_s = - \frac{e}{mc} \left[\frac{1}{1+\gamma} \frac{\vec{v}}{c} \times \vec{E}' + \frac{g}{2\gamma} \vec{B}' + \frac{f}{2\gamma} \vec{E}' \right] , \tag{2.4}$$

where $\vec{E}'$ and $\vec{B}'$ are the electric and magnetic fields in the rest frame of the particle. The first term on the right hand side of (2.4) is the familiar Thomas precession [26], the second is the precession of the magnetic dipole moment about the rest frame magnetic field ($1/\gamma$ is the time dilation factor), and the third is the precession of the electric dipole moment about the rest frame electric field.

In terms of the laboratory fields $\vec{E}$ and $\vec{B}$

$$\vec{E}' = \gamma(\vec{E} + \frac{\vec{v}}{c} \times \vec{B}) - \frac{\gamma - 1}{v^2} \vec{v} \cdot \vec{E}\, \vec{v} , \tag{2.5}$$

and

$$\vec{B}' = \gamma(\vec{B} - \frac{\vec{v}}{c} \times \vec{E}) - \frac{\gamma - 1}{v^2} \vec{v} \cdot \vec{B}\, \vec{v} . \tag{2.6}$$

Substituting Equations (2.5) and (2.6) into (2.4) the spin precession frequency in terms of the laboratory fields is found:

$$\vec{\omega}_s = -\frac{e}{mc}\left[\frac{\vec{B}}{\gamma} - \frac{1}{1+\gamma}\frac{\vec{v}}{c}\times\vec{E} + \left(\frac{g}{2}-1\right)\left(\vec{B} - \frac{\gamma}{\gamma+1}\vec{v}\cdot\vec{B}\frac{\vec{v}}{c^2}\right.\right.$$

$$\left.\left. - \frac{\vec{v}}{c}\times\vec{E}\right) + \frac{f}{2}\left(\vec{E} - \frac{\gamma}{\gamma+1}\vec{v}\cdot\vec{E}\frac{\vec{v}}{c^2} + \frac{\vec{v}}{c}\times\vec{B}\right)\right] \qquad (2.7)$$

This is the same result as obtained by Ford [28] for the expectation value of the spin flip frequency of a spin 1/2 quantum particle.

It is interesting to note that the g-factor anomaly, $a = (g/2 - 1)$, appears in (2.7) as a result of combining the effects of Thomas precession and magnetic precession. Also, for a Dirac particle ($g = 2$, $f = 0$) in a magnetic field ($\vec{E} = 0$), the Thomas precession and magnetic precession combine to give an observed precession equal to the relativistic cyclotron frequency (ω_c). For $\vec{v}$ perpendicular to $\vec{B}$ the magnitudes of the effects are

$$\text{Thomas precession} = (1-\gamma)\omega_c \quad , \qquad (2.8)$$

$$\text{magnetic precession} = \gamma\omega_c \quad . \qquad (2.9)$$

Therefore, in the present experiment ($\gamma \simeq 1.2$) the Thomas precession accounts for about 20% of the total precession.

Equation (2.7) may be simplified by making several assumptions which are consistent with the fields and orbital parameters of the present experiment. Cylindrical coordinates with the z axis along the magnetic field are most convenient:

$$\vec{B} = B_r\,\hat{r} + B_\theta\,\hat{\theta} + B_z\,\hat{z} \quad , \qquad (2.10a)$$

$$\vec{E} = E_r \hat{r} + E_\theta \hat{\theta} + E_z \hat{z} , \qquad (2.10b)$$

$$\vec{v} = v_r \hat{r} + v_\theta \hat{\theta} + v_z \hat{z} , \qquad (2.10c)$$

where $\hat{r}$, $\hat{\theta}$, and $\hat{z}$ are orthogonal unit vectors. The fields, velocities and frequencies used above are functions of space and time. However, the quantities of interest in this experiment are the fields, velocities and frequencies averaged over the trapping time. If Equations (2.10) are inserted into (2.7) and all terms are averaged over the trapping time, the following approximations can be used to eliminate terms: the bars indicate averaged quantities.

1. $\bar{v}_r = 0$. The time-averaged radial velocity must be zero if the particle is to remain trapped.
2. $\bar{v}_z = 0$. The time-averaged axial velocity is the distance between targets divided by the trapping time and is completely negligible.
3. $\overline{v_z^2} < 10^{-4}c^2$. This quantity is calculated in Section 4.2 from measurements of the magnetic field.
4. $|\bar{E}_\theta| < 10^{-7} \bar{B}_z$, otherwise electrons would lose or gain enough energy to escape detection.
5. $|\bar{E}_r|$ and $|\bar{E}_z| < 10^{-6}\bar{B}_z$. This estimated upper limit is subject to experimental verification.
6. $|\bar{B}_r| < 2 \times 10^{-6}\bar{B}_z$. In order for the electrons to stay in the trap, the axial Lorentz force must average to zero. So,

$$\bar{B}_r = \frac{c}{v_\theta} \bar{E}_z \quad .$$

7. $\bar{B}_\theta = 0$. There are no axial currents inside the beam radius.
8. $|f| < 10^{-4}$. The results of g-Factor II can be interpreted to give this limit.

Omiting terms smaller than $\bar{B}_z e/mc \times 10^{-8}$ Equation (2.7) becomes

$$\overline{\vec{\omega}_s} = -\frac{e}{mc}\left[\frac{\bar{B}_z}{\gamma} + \frac{1}{1+\gamma}\frac{\overline{v_\theta E_r}}{c} + a\bar{B}_z - \frac{a\gamma\overline{v_z^2 B_z}}{(\gamma+1)c^2}\right]\hat{z}$$

$$-\frac{e}{mc}\left[\frac{\bar{B}_r}{\gamma} - \frac{1}{1+\gamma}\frac{\overline{v_\theta E_z}}{c} + \frac{f}{2}\frac{\overline{v_\theta B_z}}{c}\right]\hat{r} \quad . \tag{2.11}$$

Since B_z varies by less than 0.1% over the trap and v_θ differs from v at most by 0.02%, the following approximations are sufficiently good:

$$\overline{v_z^2 B_z} = \overline{v_z^2}\,\overline{B_z} \quad , \qquad \frac{\overline{v_\theta B_z}}{c} = \beta\,\overline{B_z} \quad ,$$

and (2.12)

$$\frac{\overline{v_\theta E_r}}{c} = \beta\,\bar{E}_r \quad , \qquad c\,\frac{\bar{E}_r}{v_\theta} = \frac{1}{\beta}\,\overline{E_r} \quad .$$

The cyclotron frequency of the orbital motion is also subject to the above approximations. It is easily shown that

$$\overline{\vec{\omega}_c} = -\frac{e}{mc}\left[\frac{\bar{B}_z}{\gamma} + \frac{1}{\beta\gamma}\overline{E_r}\right]\hat{z} \quad . \tag{2.13}$$

The difference frequency is found by subtracting Equation (2.13) from Equation (2.11). The magnitude of the difference frequency is the measured quantity and, dropping terms smaller than $\overline{\omega_o} \times 10^{-8}$, this magnitude is found to be

$$\omega_D = \overline{\omega_o}\sqrt{\left[a - \frac{1-\beta^2}{\beta}\frac{\overline{E_r}}{\bar{B}_z} - \frac{a\gamma}{\gamma+1}\frac{\overline{v_z^2}}{c^2}\right]^2 + \left[\frac{f}{2}\beta\right]^2} \quad , \tag{2.14}$$

where $\overline{\omega_o} = -e\bar{B}_z/mc$. The terms involving $\bar{E}_r, \overline{v_z^2}$, and f are less than 0.1% of "a" over the range of β used in this experiment, thus

$$\frac{\omega_D}{\omega_o} = a - \frac{a\gamma}{\gamma+1}\frac{\overline{v_z^2}}{c^2} - \frac{1-\beta^2}{\beta}\frac{\overline{E_r}}{\overline{B_z}} + \frac{f^2\beta^2}{8a}, \qquad (2.15)$$

is a sufficiently good approximation.

Equation (2.15) has the same form as (1.11) of Case and Mendlowitz except that three correction terms are added to account for the finite pitch of the trapped beam, possible radial electric fields, and a possible electric dipole moment for the electron. The pitch correction term is calculated from the magnetic field map in Section 4.2. The magnitudes of the other two correction terms are estimated by studying the energy dependence of the measured quantity $\omega_D/k\bar{v}_o$.

III. APPARATUS

3.1. Design Criteria

Upon completion of the g-factor II experiment it was felt that the accuracy could be improved, perhaps by a factor of 10, by making several important refinements in apparatus. The g-Factor II apparatus was dismantled and the experiment completely rebuilt, for two reasons. (1) Much of the electronics was of a highly transitory nature resulting in too much down-time for maintenance. (2) The geometry of the solenoid (20 feet long and 1 foot in diameter) made the trapping and counting equipment almost inaccessible. The elimination of these two nuisances has proven to be well worth the effort. Precision, reliability, and versatility, therefore, became the design criteria for the new apparatus.

3.2. Physical Layout

The general layout of the laboratory is shown in the Frontispiece. Physically the apparatus consists of an aluminum vacuum tank approximately 18 feet long over which a solenoid 8 feet long is free to move. An ion pump is connected to one end of the tank (extreme left of Frontispiece) and a glass jar which insulates the electron gun from the tank is connected to the other end. The glass jar and all equipment riding at the gun potential are surrounded by an aluminum wire cage (extreme right side of Frontispiece). The actual experiment takes place in a region about 3 feet long near the center of the solenoid: the long vacuum tube is needed to isolate the trapping region from the iron vacuum pumps. The associated electronics is shown in the background of the Frontispiece.

3.3. Vacuum System

The vacuum tank is partitioned into two containers by an aluminum baffle plate immediately to the gun side of the trapping region (see Figure 3). A small hole in the plate allows the electron beam to pass through to the polarizing target. Oil diffusion pumps are used on the gun side of the partition and the relatively clean ion pump is used on the trapping region side. An externally operated valve in the baffle plate allows the ion pump to be roughed out through a cold trap on the oil pumps. With the machine in operation the pressures in the gun section and in the ion pump are about 8×10^{-7} mm of Hg and 5×10^{-8} mm of Hg respectively. This gives a pressure of about 2×10^{-7} mm of Hg in the trapping region.

3.4. Magnetic Field

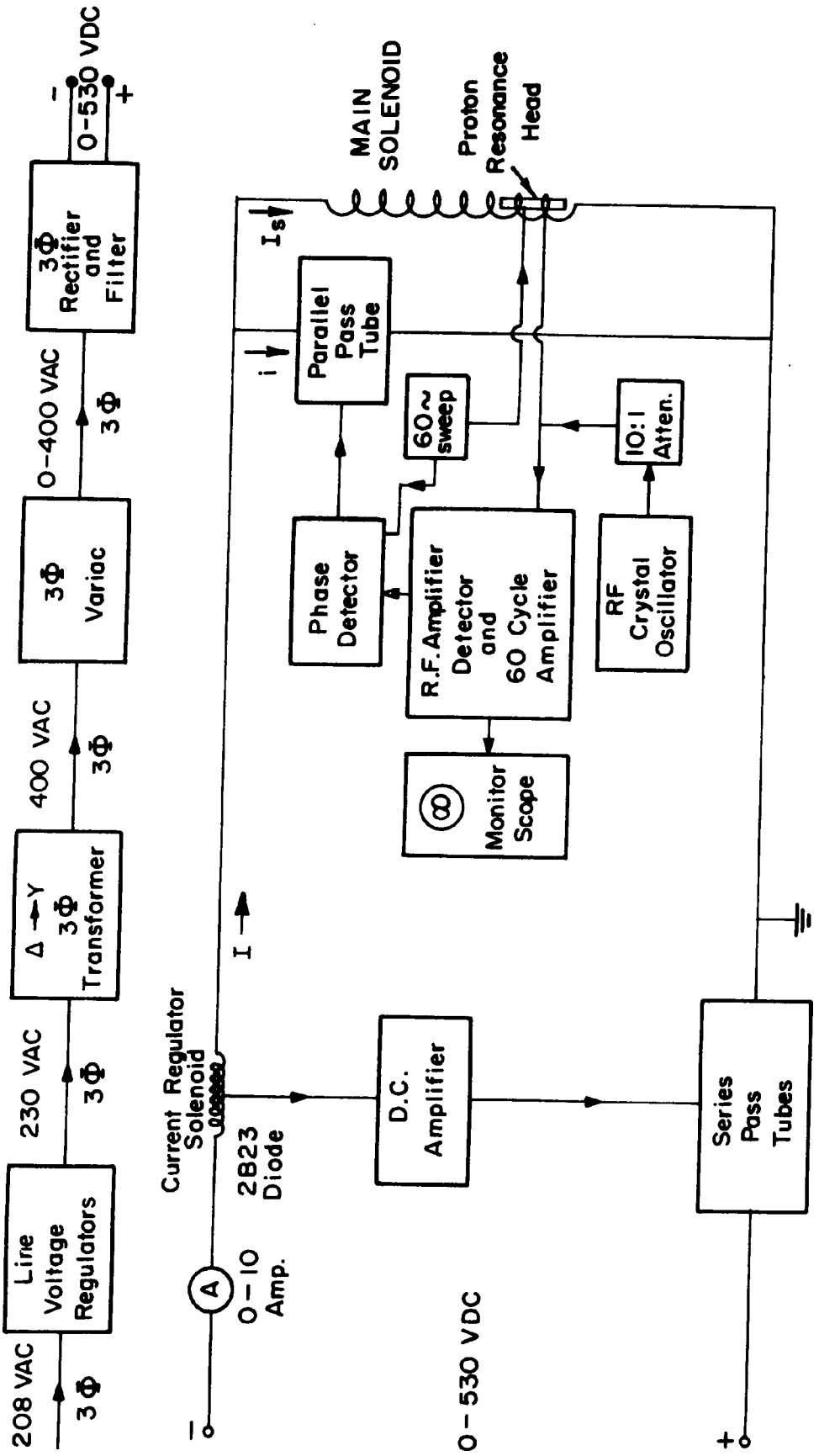
The magnetic field is produced by a solenoid wound on an aluminum spool 8 feet long and two feet in diameter. Eight layers of number 10 SCHF magnet wire produce the main solenoid field. Two-layer end-correction coils about 17 inches long are wound on each end of the main winding and are connected in series with it.

The correction coil lengths were calculated with the aid of an IBM 704 digital computer. The computer was programmed to add turns to the correction coils until the axial magnetic field, on a cylinder 7.62 cm in radius and 70 cm long at the center of the solenoid, was as uniform as possible. Fortunately, the real correction coils slightly over-correct the main solenoid field and give a weak magnetic bottle in the trapping region. The resulting magnetic well (see Figure 11) is sufficiently deep to give reasonable numbers of electrons in the trap. The measurement and analysis of the magnetic field are discussed in Section 4.1.

A block diagram of the power supply and regulators for the solenoid current is shown in Figure 8. Three Superior EMT 4207 regulators give ± 1% voltage regulation of the main three phase power line. The voltage of each phase is sensed and controlled individually. The delta-wye transformer steps up the voltage and isolates the solenoid power supply from ground. The variac, three phase rectifier, and LC ripple filter complete the power supply which is capable of delivering 10 amps at 530 volts DC. The remainder of the magnetic field regulation is accomplished in two steps. (1) A coarse series regulator which senses and controls the current I in Figure 8. (2) A fine parallel regulator senses the magnetic field and controls the small fraction of I which bypasses the solenoid.

The coarse regulator senses the current I by means of a GE 2B23 diode for which the plate current is a function of the magnetic field along the axis of the tube. The diode is mounted on the axis of a small solenoid carrying the current I. The sensor output is compared to a reference voltage in a high gain difference amplifier and the amplified error signal is applied to the grids of thirty 6AS7 pass tubes connected in parallel. The main functions of this regulator are to reduce drift and transients to levels which can be handled by the fine regulator and to reduce power supply ripple. Transients and ripple are reduced to 2% and drift is less than 0.05% per day after a 30 minute warm-up period. Power supply ripple is virtually eliminated from the magnetic field by eddy currents in the aluminum solenoid form.

The fine regulator uses a proton resonance head to sense the magnetic field inside the solenoid. The head consists of a 21 cc sample of 0.1 molar cupric chloride solution inside of an rf coil 4 cm long and 2 cm in diameter wound with No. 34 wire. This coil is mounted between two



MAGNETIC FIELD REGULATORS

Figure 8

sweep coils 7 cm in diameter and connected in series. The r-f coil is connected across a variable capacitor by about one meter of coaxial cable forming a resonant circuit with a Q of about 50. This tank circuit is driven through a 10:1 attenuator from a crystal controlled oscillator.[1] This method of excitation permits a very high oscillator Q for frequency stability, and a tank circuit Q low enough to pass the resonance signal side bands. The crystal controlled oscillator operates class A for amplitude stability and delivers between 5 and 10 volts peak-to-peak to the attenuator. Any of nine oven mounted crystals can be selected in a frequency range from 400 kc to 690 kc, corresponding to magnetic fields at the regulator head between 94 gauss and 162 gauss. After a 60 minute warm-up period the oscillator frequency is stable to $\pm$ 2 parts per million.

The tank circuit is in the grid circuit of an r-f amplifier with a gain of 25. Absorption and dispersion effects by the protons in the sample give approximately 30 microvolts of modulation on the r-f appearing at the grid. The most important sources of noise seem to be microphonics and 60 cps pickup in the head and in the r-f amplifier. The r-f amplifier is followed by a diode detector and an audio amplifier with a gain of 1000. Noise originating in these stages is negligible. Finally, a tuned 60 cps amplifier (twin T type) with a Q of about 30 narrows the system bandwidth and gives an overall signal to noise ratio of about 5:1.

The output of the 60 cps amplifier is compared to the 60 cps sweeping voltage in a phase detector to give an error voltage which controls the current in the parallel pass tube (Figure 8). With the fine

---

[1] A Pound-Knight [28] oscillator was tried, using a crystal in the feedback path as described by Blume [29]. However, the high Q and rather low frequency of the crystals give a circuit bandwidth too narrow to pass the resonance signal.

regulator locked onto the resonance line the main component of the signal from the 60 cps amplifier is 120 cps. Figure 10c shows a picture of the Lissajous pattern formed when this signal is compared to the 60 cps sweeping voltage. In this state the error signal is zero. A perturbation of the magnetic field causes a large 60 cps component to appear in the Lissajous pattern. The phase of this component depends on the sign of the perturbation and its amplitude depends on the magnitude of the perturbation. The phase detector converts this 60 cps component into a D.C. error signal whose sign and magnitude give a new solenoid current opposing the perturbation of the magnetic field.

The fine regulator has a 5 second time constant, chosen to minimize the effect of noise transients generated internally. Its primary functions are to hold the magnetic field constant over long periods of time and to assure reproducibility of the field. Infrequent power line transients are observed on the monitor scope but they are of short duration and rarely cause the fine regulator to lose control. Drift of the magnetic field has been measured and is less than 10 parts per million per day.

3.5. Timing System

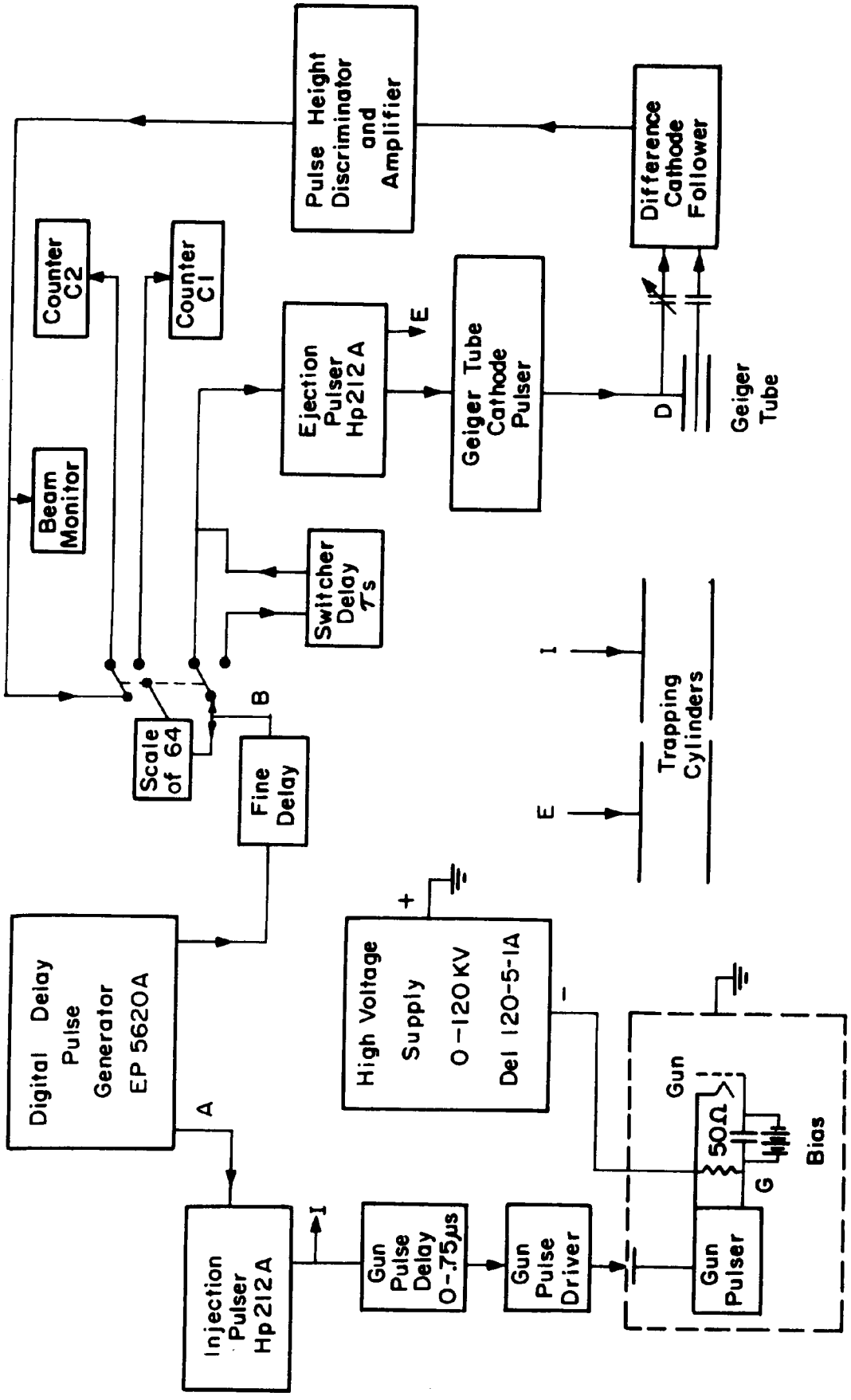
A block diagram of the timing system is shown in Figure 9. The heart of the system is an Electro-Pulse 5620A digital delay generator. It provides two pulses whose spacing can be varied from 1 to 10,000 microseconds in 1 microsecond steps. A crystal oven has been added to the standard clock oscillator to provide additional frequency stability. The clock rate has been measured by comparing it to WWV with a frequency counter.

The details of Figure 9 will be covered in Sections 3.7 and 3.6. However, a sequence of events is given here. (1) Pulse A triggers the injection pulser which applies negative 70 volts to cylinder I. (2) The gun is pulsed giving a helical beam in the trapping region. (3) The voltage is removed from cylinder I, thus trapping electrons. The timing of this event is critical and controlled by the gun pulse delay line in Figure 9. (4) After the selected trapping time, pulse B triggers the ejection pulser which applies a negative voltage to cylinder E, thus, ejecting electrons in the direction of the Geiger tube. At the same time a pulse has activated the Geiger tube, so that if an electron is scattered into it, a count is registered. (5) Ejection and Geiger tube voltages are removed and the machine is ready for another cycle. The normal repetition rate is 500 cps.

3.6. Electron Source

The electron source is an electron gun of conventional design, driven by a high voltage supply, a filament supply, and a grid pulser. The gun, the high voltage supply, and the gun pulser are shown schematically in Figure 9. The system is capable of delivering 100 milliamps peak current, or 10 microamps average current, to the polarizing target. Electrostatic focusing was achieved by empirically shaping the nose of the gun.

The high voltage supply is a Del Model 120-5-1A (120 KV and 5 milliamps). Regulation is achieved by sampling the output through a 1,000 megohm resistor and feeding this information to a Sorensen Model 1001 line voltage regulator, which in turn countrols the input voltage to the high voltage supply. The coupling from the bleeder resistor to



TIMING SYSTEM

Figure 9

the Sorensen consists of a DC amplifier and an Acromag magnetic amplifier built specially for this application. The regulator is unable to eliminate power supply ripple and corona spikes, but these have been measured and are less than 0.2% and 2.5%, respectively. After a 30 minute warm-up period, the regulator holds the DC component drift to less than 0.1% per day.

The gun filament is a spiral of 0.02 inch thoriated tungsten wire. Maximum emission occurs at a filament current of about 18 amps. An isolation transformer, capable of withstanding 130 KVDC, supplies 60 cps line voltage to the filament and gun pulser power supplies which ride at the gun potential. The filament is mounted inside of a cylindrical cooling jacket through which water is circulated. The grid pulser is a line-controlled thyratron pulser which is capable of delivering a positive 4 KV pulse, 0.2 microseconds wide, to the gun grid. Grid pulse jitter with respect to pulse A (Figure 9) is less than $\pm$ 0.01 microseconds. The grid is biased well below gun cutoff by a battery to assure gun current only during the grid pulse. Both filament current and grid pulse height can be controlled from knobs at ground potential.

3.7. Counting System

A Geiger tube is used to detect electrons scattered from the analyzing target. A curved slit system with an aperture of 2.5 mm allows only electrons in a small range of energy and scattering angle to enter the tube. The slit system reduces background (no analyzing target) to less than 1% of the normal counting rate (analyzing target in). Nelson and Pidd [30] have measured the angular dependence of the Mott asymmetry. Using their results, the slit system was designed for a scattering angle

of 110° with the incident direction. This angle should give nearly the maximum asymmetry.

An insulated brass cylinder around the center wire of the Geiger tube serves as a cathode and is pulsed to negative 100 volts for about 1 microsecond when counts are sought. A positive DC voltage is applied to the center wire which is just sufficient to make counts appear during the pulsed intervals. The Geiger pulses, appearing on the center wire, are superimposed on the cathode pulses which couple through the Geiger tube capacity. The cathode pulses are subtracted off in a difference cathode follower by adjusting the variable capacitor in Figure 9.

The advantages in using a single counter to analyze the polarization are listed in Section 1.2. The remainder of this section explains the single counter scheme. In the two counter scheme the counting rate of each counter is periodic with trapping time and has period τ_D. However, the counting rates of the two counters are 180° out of phase. That is, at trapping time t if G_1 (Figure 2) is maximum, G_2 is minimum, furthermore, at trapping time $t + \tau_{D/2}$ G_1 is minimum and G_2 is maximum. Therefore, G_1 may be replaced by a counter in the same position as G_2 if the electrons which it counts are in the trap $\tau_{D/2}$ microseconds longer than those counted by G_2. Figure 9 shows how this is accomplished, using a single Geiger tube and slit system. An electronic switch alternately (every 64 machine cycles) switches the trapping time from t to $t + \tau_s$ and simultaneously switches the output of the Geiger tube into two different scalers C_1 and C_2. C_2 records counts occurring at trapping time t, and C_1 records counts occurring at trapping time $t + \tau_s$. If $\tau_s = \tau_{D/2}$, the scaler C_1 gets the same number of counts as it would if counting the output from a Geiger tube on the opposite side of the analyzing target at

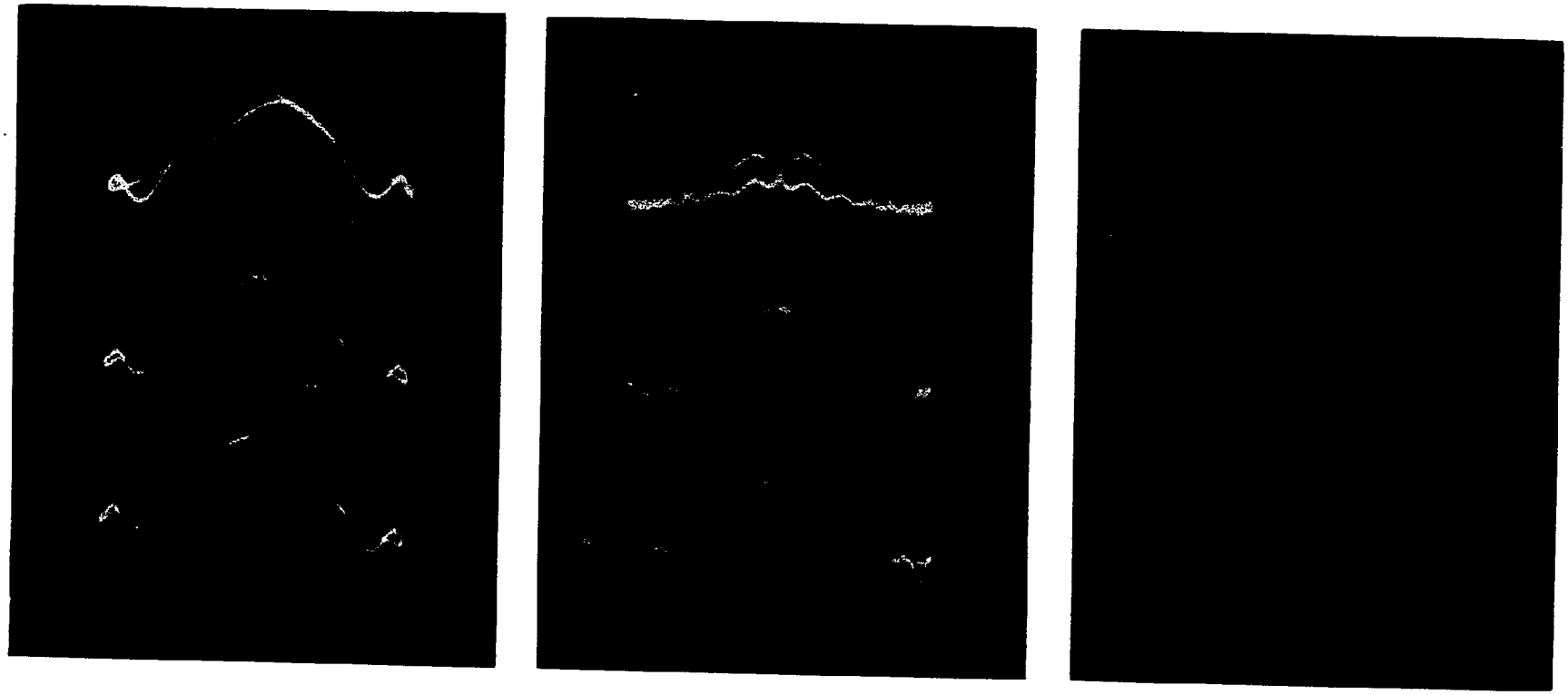
trapping time t. If τ_s is not exactly equal to $\tau_{D/2}$ the amplitude of the asymmetry is smaller and the overall phase is shifted slightly. The value of τ_s may differ from $\tau_{D/2}$ by as much as $\pm$ 50% without decreasing the asymmetry amplitude by more than 30%. Overall phase is not important because zero trapping time is not used. The switching period is short enough to prevent drifts in the counting rate from biasing the asymmetry.

IV. EXPERIMENTAL RESULTS AND ANALYSIS

4.1. Measurement and Analysis of the Magnetic Field

The magnetic field in the trapping region was mapped with a proton resonance head similar to the one described in Section 3.4. A Pound-Knight [28] type circuit was found to give the best combination of sensitivity and versatility. The resonant frequency was measured by a frequency counter which had been calibrated with WWV. The surprisingly good accuracy to which the magnetic field could be measured is indicated in Figure 10(a). These are pictures of the resonance patterns used to measure the magnetic field. The center picture was taken at a frequency of 549,721 cps: note the high signal to noise ratio and the excellent symmetry about the center. The top and bottom pictures show the patterns with the oscillator frequency changed by $\pm$ 10 cps, respectively. Actual measurements were made well within these limits, giving a maximum error per measurement of $\pm$ 10 cps or about $\pm$ 20 ppm. The measured value, of course, corresponds to the average magnetic field in the volume of the sample. Near the ends of the trapping region the field inhomogeneity is about 40 ppm over the sample volume (see Figure 11). Figure 10(b) shows the resonance line for higher amplitudes of sweeping field. The large number of wiggles indicates the high homogeneity of the field in the trapping region.

The fine magnetic field regulator was subject to systematic shifts due to stray 60 cycle pickup and slight detuning of the regulator resonance tank circuit. Therefore, a third proton resonance head, called the Monitor, was permanently mounted just outside the trapping region and used to calibrate the regulator during the measurement of the field and during the asymmetry runs.



(a)

Resonance patterns used to measure the magnetic field.
Top: f = 549,731 cps.
Middle: f = 549,721 cps.
Bottom: f = 549,711 cps.
Sweep = 0.05 gauss.

(b)

Resonance patterns for larger sweep amplitudes.
Top: Sweep = 0.5 gauss.
Middle: Sweep = 0.2 gauss.
Bottom: Sweep = 0.1 gauss.

(c)

The resonance pattern for the fine magnetic field regulator.

Figure 10. Proton Resonance Patterns.

The magnetic field was mapped several times with the solenoid moved then replaced and the regulator detuned and retuned between mappings. The reproducibility of measurements was found to be very good. The raw data for two such runs are tabulated in Appendix A1. The field is averaged over azimuth and compared to the field at the Monitor head. Figure 11 shows a plot of the ratio of the magnetic field in the trapping region to the magnetic field at the Monitor head.

The time-averaged magnetic field which the electron experiences while in the trap must be calculated as accurately as possible because the uncertainty in this quantity limits the ultimate accuracy of the experiment. Therefore, we wish to find

$$\bar{B}_z(z_1,z_2) = \frac{2}{T(z_1,z_2)} \int_{z_1}^{z_2} B_z dt = \frac{2}{T(z_1,z_2)} \int_{z_1}^{z_2} \frac{B_z}{v_z} \, dz \ , \quad (4.1)$$

where $\bar{B}_z\ (z_1,z_2)$ is the time-averaged field experienced by an electron which oscillates between z_1 and z_2 in the trap. $T(z_1,z_2)$ is the period of the oscillation and v_z is the instantaneous axial velocity in the trap. The latter quantity is found from the axial energy relationship

$$\frac{1}{2} m v_z^2 = \frac{e v_\theta}{c} \int_{z_1}^{z} B_r dz \ , \quad (4.2)$$

where v_θ is taken outside the integral because it varies by less than 0.02% over the trapping region. Since B_z, and not B_r, is the measured quantity,[2] (4.2) must be expressed in terms of B_z. In Appendix C3, it is shown that in the trapping region the following relationship is good to 1 part in 20:

---

[2]Actually $\sqrt{B_z^2 + B_r^2}$ is measured, but this differs from B_z by less than 1 part in 10^7 in the trapping region.

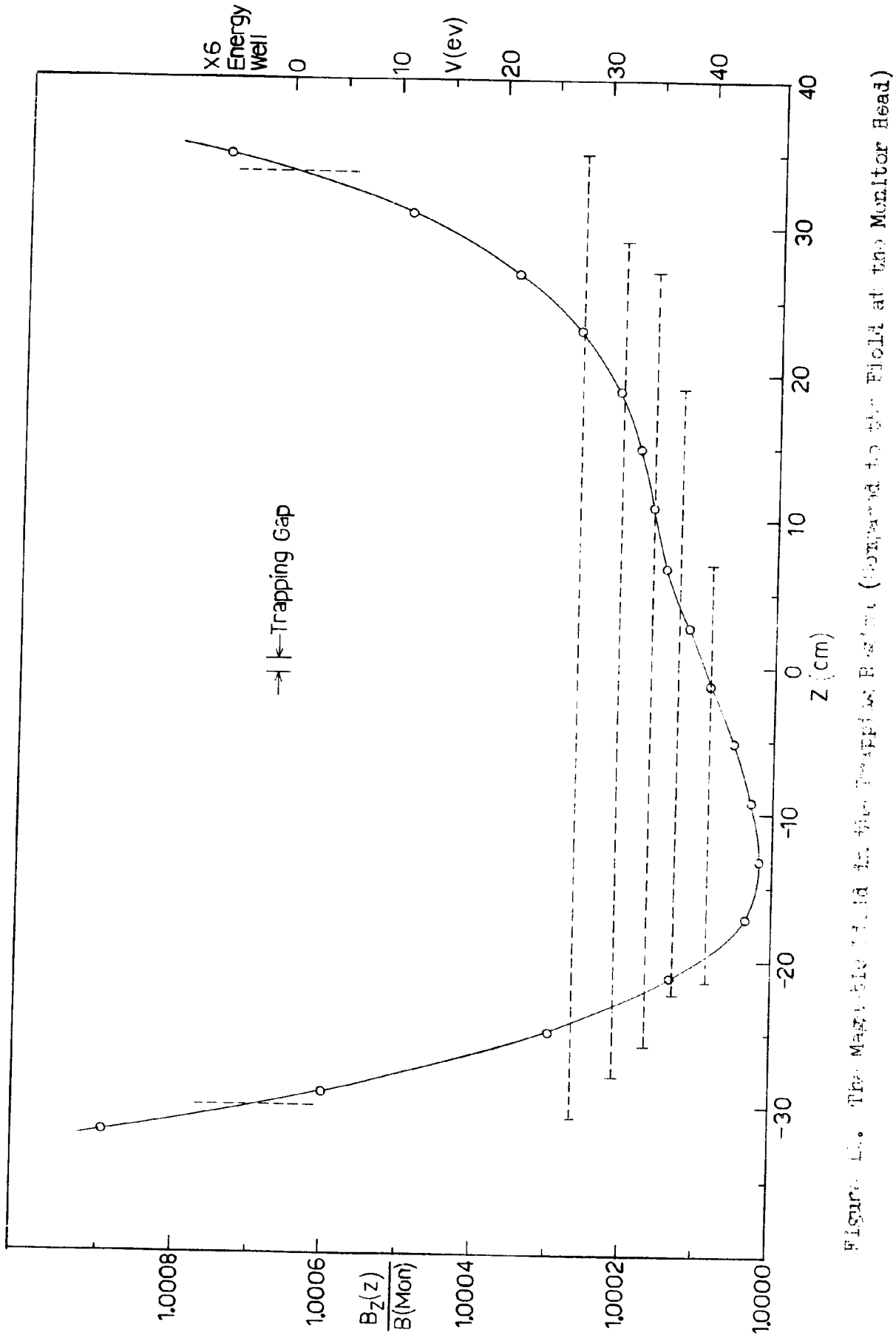


Figure 4.6 The Magnetic Field in the Trapping Region (Compared to the Field at the Monitor Head)

$$\int_{z_1}^{z} B_r dz = -\frac{R}{2}\left[B_z(z) - B_z(z_1)\right] \quad , \tag{4.3}$$

for points at the beam radius, R. Substituting (4.3) into (4.2), one obtains the instantaneous axial velocity of an electron which is trapped between z_1 and z_2:

$$v_z = \sqrt{\frac{ev_\theta R}{mc}\left[B_z(z_1) - B\ (z)\right]} \quad . \tag{4.4}$$

The quantity z_2 is found from (4.4) by setting $z = z_2$ and $v_z = 0$:

$$B_z(z_1) = B_z(z_2) \tag{4.5}$$

Thus, the axial velocity of electrons, trapped with any specified amplitude (z_1), has been expressed in terms of measured quantities.

The period, $T(z_1,z_2)$, for electrons with amplitude z_1 is given by

$$T(z_1,z_2) = 2\int_{z_1}^{z_2} \frac{dz}{v_z} = 2\sqrt{\frac{mc}{ev_\theta R}} \int_{z_1}^{z_2} \frac{dz}{\sqrt{B_z(z_1) - B_z(z)}} \quad . \tag{4.6}$$

Substituting Equations (4.6) and (4.4) into (4.1) and simplifying the result one gets,

$$\overline{B_z}(z_1) = B_z(z_1) - \frac{\int_{z_1}^{z_2} \sqrt{B_z(z_1) - B_z(z)}\, dz}{\int_{z_1}^{z_2} \frac{dz}{\sqrt{B_z(z_1) - B_z(z)}}} \quad . \tag{4.7}$$

Therefore, the time-averaged magnetic field, experienced by trapped electrons with amplitude z_1, can be found from (4.7) by integrating functions of the measured magnetic field. These integrals have been performed graphically for the magnetic field shown in Figure 11. Five amplitudes were

chosen: 35 cm, 31 cm, 27 cm, 19 cm and 7 cm. The results are shown on Figure 11 as horizontal dashed lines which terminate at the corresponding values of z_1 and z_2. The values of the square root in (4.7) are tabulated in Appendix A2.

The maximum amplitude in the trap is indicated in Figure 11 by a vertical dashed line at 33.7 cm. This represents the end of the trapping cylinder and the leading edge of the analyzing target. Equation (4.5) then gives the maximum amplitude on the left of the trap as -30 cm. Due to the slight axial asymmetry of the magnetic field the minimum possible amplitude is about 5 cm. Therefore, the time-averaged magnetic field, experienced by an electron having any possible amplitude in the trap, must be within the following limits:

$$1.000\ 08 < \frac{\overline{B_z}}{B(\mathrm{Mon})} < 1.000\ 26 \quad . \tag{4.8}$$

This range can be reduced considerably by making use of some experimental results. For low ejection pulse voltages, only electrons with large amplitudes in the trap will be given enough axial energy to reach the analyzing target. As the ejection voltage is increased from zero, counts begin to appear at 1 volt. This means that there are certainly electrons trapped with nearly the maximum amplitude. As the ejection voltage is increased further, a maximum counting rate is reached. The ejection voltage, corresponding to this maximum, is a measure of the lowest energy level to which the magnetic well is populated.

The energy level, corresponding to a given amplitude z_1, is given by

$$V(z_1) = -\int_{33.7}^{z_1} B_r e v_\theta dz \quad , \tag{4.9}$$

where the maximum amplitude in the well has been arbitrarily assigned the energy level zero. Equation (4.3) is then used to get

$$V(z_1) = -\frac{1}{2} e v_\theta R \left[B_z(33.7) - B_z(z_1) \right] \quad . \tag{4.10}$$

Therefore, the energy well has the same shape as the magnetic field map. For example, the energy scale on the right of Figure 11 corresponds to 81 kilovolt electrons in a magnetic field of about 129 gauss. Using (4.10), we can calculate an energy scale for the well of any given setting of the electron energy and magnetic field.

The final data of this experiment was taken at four different settings of energy and magnetic field. The values of these settings are given in Appendix C4. Hereafter, they are referred to as X3, X6, X8, and X9 (denoting the number of the crystal to which the magnetic field is locked). The energy scale for each of these four settings has been determined from (4.10) and the maximum well depth is given in Appendix C4. Counting rate as a function of ejection voltage has been studied for each of the four settings and the ejection voltage corresponding to the measured maximum was used in the final data runs.

Thus, by using an ejection voltage less than the maximum well depth, electrons in the bottom of the well (i.e., electrons trapped with small amplitudes) are not ejected to the analyzing target. The ejection voltages used in the final data runs and the corresponding minimum amplitudes for each setting are given in Appendix C4. The range of possible time-averaged magnetic fields expressed by (4.8) includes all well levels.

This range has been narrowed considerably by rejecting electrons in the bottom of the well. The time-averaged magnetic field for each of the four settings, at which final data was taken, becomes

$$\frac{\overline{B_z}}{B(\text{Mon})} = \begin{array}{ll} 1.000\ 22 \pm 0.000\ 04 & \text{for X3}, \\ 1.000\ 21 \pm 0.000\ 05 & \text{for X6}, \\ 1.000\ 20 \pm 0.000\ 06 & \text{for X8}, \\ 1.000\ 20 \pm 0.000\ 06 & \text{for X9}, \end{array} \tag{4.11}$$

The values given in (4.11) will be used in Section 4.3 to calculate the results of this experiment.

Finally, the value of the pitch correction term which appears in (2.15) can be calculated from the magnetic field map. We wish to evaluate the time-averaged square of the axial velocity. Using Equations (4.4) and (4.6) we get

$$\overline{v_z^2} = \frac{2}{T(z_1,z_2)} \int_{z_1}^{z_2} v_z dz = \frac{ev_\theta R}{mc} \frac{\int_{z_1}^{z_2} \sqrt{B_z(z_1) - B_z(z)}\, dz}{\int_{z_1}^{z_2} \frac{dz}{\sqrt{B_2(z_1) - B_z(z)}}} . \tag{4.12}$$

The integrals in (4.12) have already been evaluated in connection with (4.7) for five different amplitudes. The value found for the pitch correction term for each of the four final data settings is

$$\frac{a\gamma}{\gamma + 1} \frac{\overline{v_z^2}}{c^2} = \begin{array}{ll} (8.0 \pm 2.0) \times 10^{-8} & \text{for X3}, \\ (4.4 \pm 1.9) \times 10^{-8} & \text{for X6}, \\ (3.2 \pm 1.9) \times 10^{-8} & \text{for X8}, \\ (2.7 \pm 1.4) \times 10^{-8} & \text{for X9}, \end{array} \tag{4.13}$$

where 0.00116 was used for "a" and the uncertainties quoted are limits of error in choosing the amplitude (z_1) in (4.12). These results are used in Section 4.3 to calculate the final result.

4.2. Measurement and Analysis of the Difference Frequency

The difference frequency ω_D appearing in Equation (2.15) is found by measuring the scattering asymmetry from the analyzing foil as a function of trapping time. The period ($\tau_D = 2\pi/\omega_D$) of the resulting cosine curve is measured by finding the trapping times corresponding to two maxima which are several hundred cycles apart. Dividing the time between these maxima by the counted number of cycles between them, one obtains the period τ_D with high accuracy.

The peak in the asymmetry, which would occur at zero trapping time, has not been used because this requires a measurement of (1) the absolute time which the electrons spend in the magnetic field and (2) the precession caused by the electric fields used in trapping. Both of these quantities are very hard to evaluate. The absolute trapping time has an inherent uncertainty due to the finite time-spread of the injected electron beam. Also, there is a lag in ejection because of the finite transit times of electrons in the trap. Finally, small circuit delays of the injection and ejection pulses could contribute sizable error. These difficulties are avoided by measuring τ_D between two measured asymmetry peaks. Then, only changes in trapping time are important and these changes are controlled by a crystal oscillator which has been calibrated against WWV. Trapping time is the only experimental parameter which is changed during an asymmetry run. Therefore, the precession caused by the electric fields used in trapping is the same for all trapping times and cancels out of the calculation of τ_D.

Since the errors in measuring the difference frequency are mostly statistical, they can be reduced by simply amassing more data. Small

error could be obtained by measuring asymmetry maxima separated by very large trapping times (up to 10 miliseconds with the present apparatus) or by taking enough data at each maximum to establish its position very accurately. However, we chose to make a number of runs (9) at each of four settings of electron energy and magnetic field and to average the results of these runs. In this way, systematic shifts due to drifting, and random errors due to adjustment of experimental parameters, are both included in the statistical error of the averaged result. The 36 runs took about five weeks to complete. The solenoid was moved and replaced, and the vacuum was cycled between Runs XXXII and XXXIII. No systematic shifts of the difference frequency were observed.

The resonant frequency of the Monitor head was measured periodically during each run. It was found to be nearly constant during the course of a run, indicating negligible drift of the magnetic field. However, due to errors in adjustment of experimental parameters, the Monitor frequency, f(Mon), differed slightly between runs of the same settings of energy and field. Thus, f(Mon) must be included in the averaging of the results of the 36 runs. The data for all 36 asymmetry runs is given in Appendix B1 and the end points of the first four runs are plotted in Figure 12.

A maximum for each end point of each run was found using an IBM 709 computer. A cosine curve was adjusted in phase, amplitude, and axis shift to give a least-squares fit to the data. The phase is, of course, the quantity of interest. The sum of the squares of the deviations was also obtained for the best fit and used to calculate a weight factor for averaging the results. The computed maxima and the weight factors are given in Appendix B2.

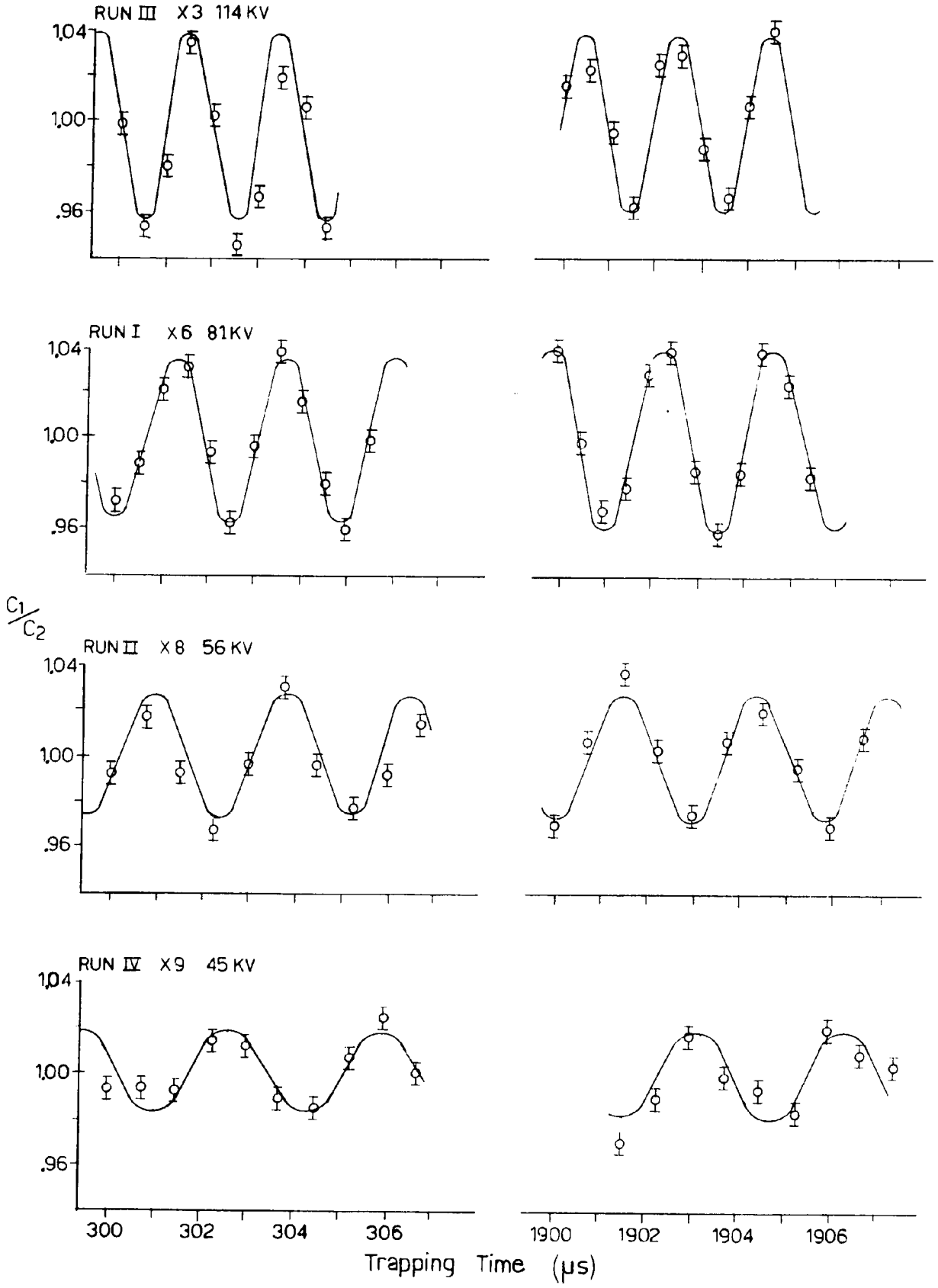


Figure 12. Data for the End Points of First Four Runs.

Counting the number of cycles between two measured peaks must be done correctly. The procedure used in counting the number of cycles for Run I is as follows. (1) The measured end-point maxima are estimated at 301.3 ± 0.1 microseconds and 1904.7 ± 0.1 microseconds. (2) The time half-way between these peaks is 1103.0 ± 0.1 microseconds and enough data was taken to establish a maximum here. Therefore, the number of cycles (N) between the end points is even. (3) Enough data was taken to find a maximum about 1/3 of the way between the end points. This peak (833.4 ± 0.1 microseconds) is used to predict a maximum at 1897.6 ± 0.3 microseconds. It, therefore, predicts the N-3 maximum and N must be divisable by 3. N has now been established to an accuracy of ± 6 cycles or about ± 1%. (4) Enough data was taken to find a maximum at 351.4 ± 0.1 microseconds. The number of cycles (n) between this maximum and 301.3 ± 0.1 microseconds can be estimated by

$$n = \frac{50.1}{2.4 \pm 0.1} = 20.8 \pm 1 \quad , \tag{4.14}$$

where the denominator is the period estimated from the data at one of the end points. (5) Enough data was taken to establish a minimum at 326.4 ± 0.1 microseconds so n is an odd number, n = 21. (6) Equation (4.14) can now be turned around to give a better estimate of the period.

$$\tau_D = \frac{50.1 \pm 0.2}{21} = 2.386\ (1 \pm 0.5\%) \quad . \tag{4.15}$$

(7) N can now be estimated to ± 0.5%:

$$N = \frac{1603.4}{2.386\ (1 \pm 0.5\%)} = 672.0 \pm 4 \quad , \tag{4.16}$$

but, since N is divisable by 2 and by 3

$$N = 672 \quad . \tag{4.17}$$

Similar procedures were followed in each of the first four runs. Statistical and random errors are about 1/10 of the error due to changing N by 1 and, therefore, the counting procedure is not necessary in subsequent runs.

The values of N and τ_D for each of the 36 runs are listed in Appendix B2. Also listed are the values of τ_D f(Mon) for each run and the weighted average of this quantity for each of the four settings of energy and magnetic field. Only one of the 36 final data runs was rejected for statistical reasons. The deviation from the mean in Run XXIII was nearly 4 times greater than the average deviation for the other 8 runs. Therefore, its results were excluded during the final averaging. The averaged results for each setting are

$$\tau_D f(\text{Mon}) = \begin{array}{ll} 1.311\ 380 + 0.000\ 025 & \text{for X3}\ , \\ 1.311\ 346 + 0.000\ 032 & \text{for X6}\ , \\ 1.311\ 277 + 0.000\ 049 & \text{for X8}\ , \\ 1.311\ 228 + 0.000\ 073 & \text{for X9}\ , \end{array} \tag{4.18}$$

where the error quoted is the weighted root-mean-square of the deviations of the results at each setting. A factor of 0.999 982 has been included in the values given in (4.18) to correct for the true frequency of the timing clock oscillator. The frequency was compared to WWV and found to be 999,982 cps, therefore, the time intervals recorded in the data are too large by 18 ppm. The values in (4.18) are used in Section 4.3 to compute the final results.

Several remarks about some features of the asymmetry data should be made. First, the maximum asymmetry obtained in this experiment was

about 5% at electron energies of 114 KV. Theoretically, the asymmetry should be twice as large (see Appendix C2). Since the amplitude of the asymmetry curve was about the same at 1900 microseconds as at 300 microseconds (see Figure 12), depolarization with trapping time is negligible. The most probable explanations are: (1) scattering from the aluminum clamp holding the polarizing target, (2) plural scattering from the analyzing target which was not carefully oriented.

Secondly, the asymmetry amplitude measured in this experiment has a much stronger energy dependence than is predicted by theory. For example, in Figure 12 the maximum asymmetry for 114 KV electrons is almost 2.5 times larger than the maximum asymmetry for 45 KV electrons. Theoretically, one would expect a factor of only 1.25 decrease in asymmetry at 45 KV. The energy dependence of current theories for depolarization from plural scattering and inelastic scattering in the targets is not sufficient to account for the observed results. These effects are being investigated further with more careful attention given to target mounting and orientation.

4.3. Results, Errors, and Conclusions

Results

The results of the two preceeding sections are used here to calculate $\omega_D/\bar{\omega}_o$ and then "a." Of the three correction terms appearing in Equation (2.15), one has already been evaluated in Section 4.1 from the magnetic field map and the other two are estimated below from the energy dependence of $\omega_D/\bar{\omega}_o$.

The quantity $\omega_D/\bar{\omega}_o$ can be expressed in terms of well-known constants and the quantities measured in this experiment:

$$\frac{\omega_D}{\bar{\omega}_o} = \frac{2\pi}{\tau_D}\frac{mc}{e\bar{B}_z} = \frac{mc}{e}\Gamma_p\frac{B(Mon)}{\bar{B}_z}\frac{1}{f(Mon)\tau_D} \quad , \tag{4.19}$$

where Γ_p is the accurately known gyromagnetic ratio for protons. The last two terms of (4.19) have been measured in this experiment and evaluated in Sections 4.1 and 4.2. The best current values [33] for the constants in (4.19) are

$$\Gamma_p = (2.675\ 13 \pm 0.000\ 02) \times 10^4 \frac{1}{\text{sec} \cdot \text{gauss}} \quad , \tag{4.20}$$

$$\frac{e}{m} = (5.273\ 05 \pm 0.000\ 07) \times 10^{17} \frac{\text{esu}}{\text{gm}} \quad , \tag{4.21}$$

and

$$c = (2.997\ 929 \pm 0.000\ 008) \times 10^{10} \frac{\text{cm}}{\text{sec}} \quad . \tag{4.22}$$

Equation (4.19) can now be written as

$$\frac{\omega_D}{\bar{\omega}_o} = (1.520\ 913 \pm 0.000\ 034) \times 10^{-3} \frac{B(Mon)}{\bar{B}_z}\frac{1}{f(Mon)\tau_D} \quad . \tag{4.23}$$

Inserting the measured values from Equations (4.11) and (4.18), one gets a value for $\omega_D/\bar{\omega}_o$ at each of the four settings of electron energy and magnetic field used in this experiment:

$$\frac{\omega_D}{\bar{\omega}_o} = \begin{array}{ll} 0.001\ 159\ 52 + 0.000\ 000\ 04 & \text{for X3} \ , \\ 0.001\ 159\ 57 + 0.000\ 000\ 05 & \text{for X6} \ , \\ 0.001\ 159\ 64 + 0.000\ 000\ 06 & \text{for X8} \ , \\ 0.001\ 159\ 68 + 0.000\ 000\ 07 & \text{for X9} \ , \end{array} \tag{4.24}$$

where the uncertainty quoted is the probable error obtained by taking the square root of the sum of the squares of the three contributing percentage errors.

We now have values for two of the five terms in Equation (2.15). These two terms are written on the right in the following rearrangement of (2.15):

$$a - \frac{1-\beta^2}{\beta}\frac{\bar{E}_r}{\bar{B}_z} + \frac{f^2\beta^2}{8a} = \frac{\omega_D}{\bar{\omega}_o} + \frac{a\gamma}{\gamma+1}\frac{\overline{v_z^2}}{c^2} \quad . \tag{4.25}$$

The terms on the right can now be replaced by their measured numerical values given by Equations (4.13) and (4.24)

$$a - \frac{1-\beta^2}{\beta}\frac{\bar{E}_r}{\bar{B}_z} + \frac{f^2\beta^2}{8a} = \begin{array}{ll} 0.001\ 159\ 60 \pm 0.000\ 000\ 05 & \text{for X3}\ , \\ 0.001\ 159\ 61 \pm 0.000\ 000\ 06 & \text{for X6}\ , \\ 0.001\ 159\ 67 \pm 0.000\ 000\ 07 & \text{for X8}\ , \\ 0.001\ 159\ 71 \pm 0.000\ 000\ 07 & \text{for X9}\ , \end{array} \tag{4.26}$$

where again the uncertainty is the probable error. Therefore, (4.26) gives the experimental results for "a" plus correction terms to account for possible radial electric fields and an electric dipole moment for the electron. There is a systematic shift of the results with energy and magnetic field. The value of β for each setting is

$$\beta = \begin{array}{ll} 0.578 & \text{for X3}\ , \\ 0.505 & \text{for X6}\ , \\ 0.433 & \text{for X8}\ , \\ 0.394 & \text{for X9}\ . \end{array} \tag{4.27}$$

Therefore, the values of (4.26) decrease for increasing β. Any contribution from the electric dipole term must cause an increase in the results as β increases. Therefore, most of the energy dependence of the results must be attributed to negative radial electric fields. For this reason, and on the basis of current electron theory, the electric dipole correction term is assumed to be negligible. Also, the value of "a" is assumed to be independent of β.

The beam radius was kept constant for all settings of energy and magnetic field, therefore, the following relationship holds for all settings:

$$\overline{B_z} = \frac{mc^2}{eR} \frac{\beta}{\sqrt{1-\beta^2}} \quad . \tag{4.28}$$

The electric field correction term in (4.26) can then be written as

$$\frac{1-\beta^2}{\beta} \frac{\overline{E}_r}{\overline{B}_z} = \frac{mc^2}{eR} \frac{\overline{E}_r}{\overline{B}_z^2} \sqrt{1-\beta^2} \quad . \tag{4.29}$$

This form is convenient because in the range of β used in this experiment (4.26) is nearly a linear function of $1/\overline{B}_z^2$. The results in (4.26) are plotted against $1/\overline{B}_z^2$ in Figure 13. The curve shown represents the least-squares fit to the weighted results. At $1/\overline{B}_z^2 = 0$ the electric field correction term goes to zero and the intersection of the fitted curve with this axis gives the measured value for "a":

$$a = 0.001\ 159\ 57 \pm 0.000\ 000\ 07 \quad , \tag{4.30}$$

where this error is the result of using the probable error from (4.26). The method of obtaining this error is explained at the end of the next part of this section. The average radial electric field experienced by electrons in the trap can also be found from the fitted curve. As expected from the weak energy dependence of the results, this field is extremely small

$$\overline{E}_r = (-1.5 \pm 1.5) \times 10^{-3} \text{ volts/cm} \quad , \tag{4.31}$$

and probably due, in part, to space charge.

The results of this experiment are now compared to those of g-Factor II. Figure 14 is similar to Figure 13 except that the vertical scale has been contracted by a factor of 10 and the fitted curve has been omitted. Also included are the results of g-Factor II and some early results of the present experiment. The factor of 30 improvement in the accuracy of the present result over that of g-Factor II is a consequence of the great reduction in the error flags and the relatively weak energy dependence of the results. The refinements in apparatus and technique which produced this improvement are listed at the end of Section 1.2.

An effort was made in the early stages of the present experiment to reproduce the results of g-Factor II. Relatively dirty brass trapping cylinders were used outside and inside the beam radius, thus, reproducing the geometry of the trapping region used in g-Factor II. The results are indicated in Figure 14 and look much like those of g-Factor II. The steeper slope of the later results is due to the smaller beam radius used in this experiment. Several similar tests were run and it was found that the slope could be reduced considerably if the surfaces of the brass cylinders were cleaned carefully. Thus, the interpretation of the results of g-Factor II was completely verified.

Errors

The error in the final result, Equation (4.30), is the result of combining many sources of error. First, there are the several experimental errors which combine to give the errors quoted in (4.26) and shown in Figure 13. Secondly, there is some error associated with fitting a curve to the results in order to account for stray radial electric fields. The experimental errors and their sources are listed and explained

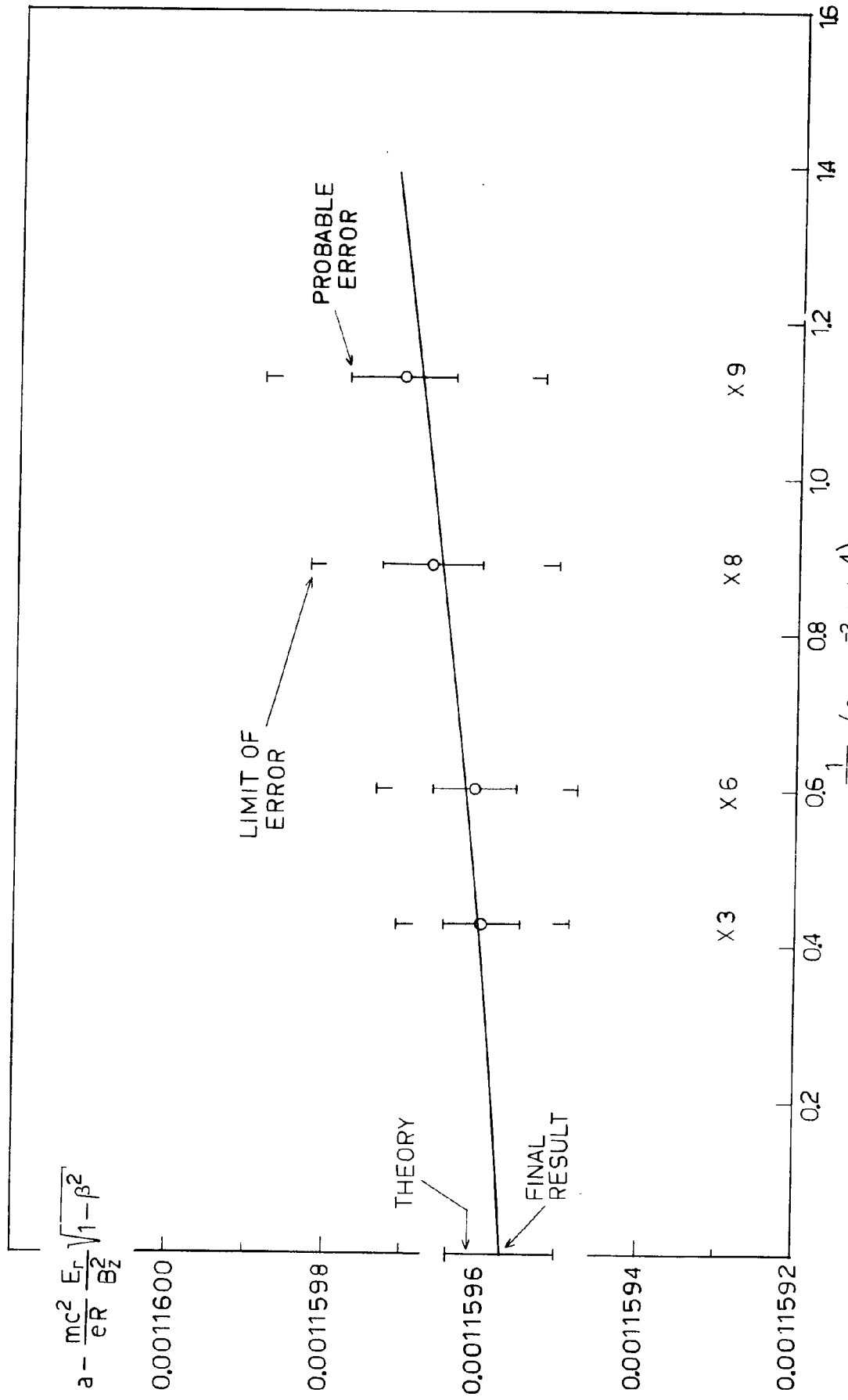


Figure 13. Evaluation of "a"

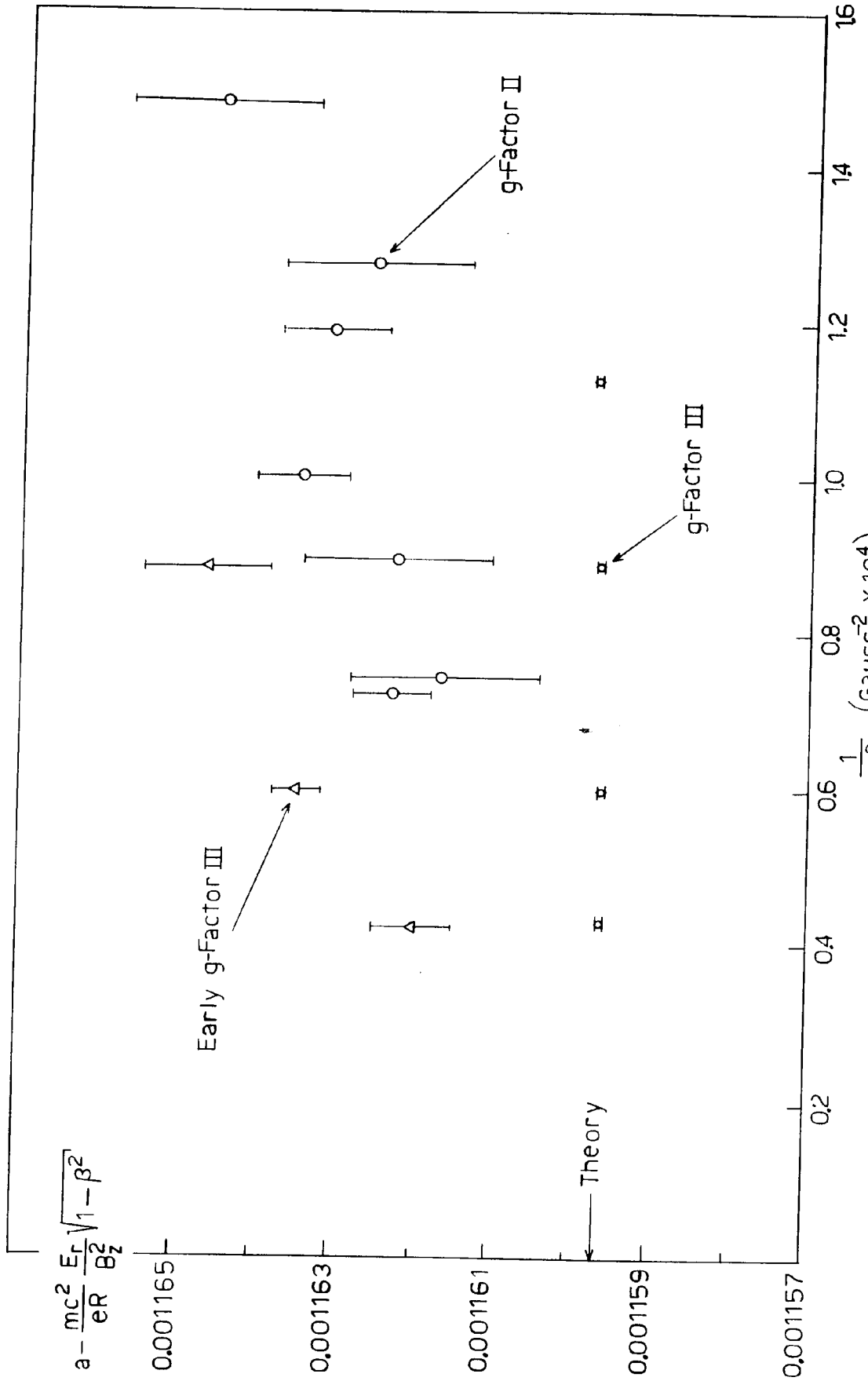


Figure 14. Comparison of Results of g-Factor II and g-Factor III

below. The error listed is the maximum percentage error which the given source could introduce into (4.26).

Source	X3	X6	X9	X10
A	40 ppm	50 ppm	60 ppm	60 ppm
B	19 ppm	24 ppm	37 ppm	56 ppm
C	7 ppm	9 ppm	11 ppm	13 ppm
D	17 ppm	16 ppm	16 ppm	12 ppm
E	23 ppm	23 ppm	23 ppm	23 ppm
Limits of Error	106 ppm	122 ppm	147 ppm	164 ppm

A. The uncertainty in assigning the average magnetic field which an electron experiences while in the trap is the ultimate limitation on the accuracy of this experiment. The error quoted in the table is due to, (1) uncertainty in assigning an average level in the potential well, (2) estimates of the accuracy of the results of mapping the magnetic field, (3) estimates of the error introduced by using (4.3) in analyzing the magnetic field in the trapping region. These errors were considered in assigning the uncertainties in (4.11).

B. Random errors in measuring τ_D are estimated by using the standard deviation of the results of nine runs at each setting of energy and magnetic field. These errors include, (1) statistical errors from the counting process, (2) errors in fitting cosine curves to the data, (3) errors due to slow drifts in regulators and changing surface conditions

on the trapping cylinders, (4) errors in reproducing the magnetic field, electron energy, and other experimental parameters. These errors enter the analysis in (4.18).

C. Uncertainties in the values assigned to f(Mon) come from two sources. (1) Experimental errors in finding the true resonance have been estimated from the symmetry of the resonance pattern (see Figure 10). (2) Slight drifts in the value of f(Mon) during the course of a run introduce an uncertainty in the value to be assigned. These errors are also included in (4.18).

D. Evaluation of the pitch correction term involves the assignment of an average energy level in the potential well. Therefore, an error is introduced due to the finite range of populated energy levels in the well. This error enters the analysis through (4.13).

E. The values of the constants used to obtain (4.23) have uncertainties which contribute to the final error.

The errors listed above represent the maximum possible experimental errors which enter into the evaluation (4.26). Their sum is the limit of experimental error and is indicated for each point in Figure 13. The error in (4.26) is the probable error obtained by combining the errors from A, B, C and E by taking the square root of the sum of the squares and then combining this result with the error from D by the same method.

The error introduced into the final result, Equation (4.30), by the uncertainty in the stray electric field is evaluated in the curve fitting process. The final value for "a" is found by fitting a curve to the weighted points in Figure 13. The limits assigned to this value are obtained by fitting a curve to an extreme value on the X3 error flag, the probable value of X6, the probable value of X8, and the opposite extreme

value on the X9 error flag. For example, if a curve is fitted to the following points:

$$\begin{array}{lll} 0.001\ 159\ 55 & \text{for} & X3\ , \\ 0.001\ 159\ 61 & \text{for} & X6\ , \\ 0.001\ 159\ 67 & \text{for} & X8\ , \\ 0.001\ 159\ 78 & \text{for} & X9\ , \end{array}$$

the resulting value of "a" is

$$a_{LO} = 0.001\ 159\ 50\ .$$

Similarly, a least-squares fit to the maximum probable value for X3, the probable value for X6, the probable value for X8, and the minimum probable value for X9 gives

$$a_{HI} = 0.001\ 159\ 64\ .$$

Therefore, the error quoted in (4.30) is associated with the probable error.

This same process has been applied to the limits of error shown in Figure 13. The resulting value for "a" is

$$a = 0.001\ 159\ 57 \pm 0.000\ 000\ 15\ , \qquad (4.32)$$

where this error must be regarded as the maximum possible error of this experiment. In the words of Professor Franken, I would be absolutely FLABBERGASTED if the value were ever proven to be outside of these limits.

Conclusions

The final result for the anomaly in the g-factor of the free electron is given by (4.30) as

$$a = 0.001\ 159\ 57 \pm 0.000\ 000\ 07 \tag{4.33}$$

where the probable error is quoted. The limit of error is given in (4.32). This is to be compared to the theoretical value given in (1.6) as

$$a = 0.001\ 159\ 61 \pm 0.000\ 000\ 01 \tag{4.34}$$

where this error is due to the uncertainty in the present value for the fine structure constant. The measured value should also be compared to the power series expansion for "a" in order to check the theoretical value for the coefficient of the α^2 term:

$$a = \frac{\alpha}{2\pi} - 0.328\frac{\alpha^2}{\pi^2} + \cdots \tag{4.35}$$

Written in this form (4.33) becomes

$$a = \frac{\alpha}{2\pi} - (0.34 \pm 0.02)\frac{\alpha^2}{\pi^2} \tag{4.36}$$

Therefore, the value of "a" measured in this experiment is in excellent agreement with the present theoretical value. This agreement must be regarded as one of the best experimental checks to date on the theory of quantum electrodynamics.

Other well-developed experiments for measuring "a" have errors larger than 20 times the error in (4.33). Therefore, until some entirely new experiment is devised, improvements in this experiment offer the best hope for a better measurement of "a." At a sacrifice in counting rate a shallower potential well and longer trapping times could be used to improve the accuracy by a factor of 2. Then one would have to deal with the error introduced by the constants e/m and Γ_p. This further improvement

does not seem worthwhile at this time. In view of these remarks g-Factor III must be regarded as a definitive experiment.

A final remark should be made concerning the possibility of an electric dipole moment for the electron. Theoretically, the electron has no EDM (f = 0): this assertion is necessary to conserve parity in the Dirac Equation. If one accepts the theoretical value for "a" as being correct, then the results of this experiment can be used to set an upper limit on the magnitude of f. In order to preserve the agreement between measured and theoretical results for "a," the electric dipole correction term in (4.25) must be smaller than 10^{-7}. This implies

$$f < 3 \times 10^{-5} \qquad (4.38)$$

and sets an upper limit on the electron EDM of

$$3 \times 10^{-16} \text{ cm (times the electron charge)} \quad . \qquad (4.38)$$

Studies are now underway on possible methods of modifying the present apparatus so that the EDM can be measured directly.

APPENDIX A1

DATA FOR TWO FIELD MAPPINGS

Map 1: f(Monitor) = 549,585 ± 5 cps

Z	Azimuth				Azimuth Average	$\frac{B_z}{B(\text{Monitor})}$
	0	$\pi/2$	π	$3\pi/2$		
35		550,005	549,989	549,986	549,993	1.000742
31		549,872	549,855	549,855	549,861	1.000502
27	549,782	549,788	549,770	549,779	549,780	1.000354
23	549,737	549,736	549,727	549,735	549,734	1.000271
19	549,711	549,705	549,696	549,706	549,704	1.000216
15	549,687	549,680	549,680	549,697	549,686	1.000183
11	549,680	549,668	549,670	549,689	549,677	1.000167
7	549,667	549,654	549,661	549,678	549,665	1.000145
3	549,654	549,637	549,644	549,657	549,648	1.000114
- 1	549,630	549,620	549,627	549,647	549,631	1.000083
- 5	549,612	549,600	549,608	549,627	549,612	1.000049
- 9	549,599	549,587	549,598	549,610	549,598	1.000023
-13	549,594	549,592	549,594	549,603	549,596	1.000020
-17	549,613	549,615	549,610	549,610	549,612	1.000049
-21	549,654	549,665	549,661	549,650	549,658	1.000132
-25	549,742	549,764	549,763	549,737	549,752	1.000303
-29	549,904	549,931	549,919	549,887	549,910	1.000591
-32	550,050	550,094	550,094	550,077	550,064	1.000871

Map 2: f(Monitor) = 549,575 ± 5

Z	Azimuth				Azimuth Average	$\frac{B_z}{B(\text{Monitor})}$
	0	$\pi/2$	π	$3\pi/2$		
35		549,997	549,984	549,977	549,986	1.000744
31		549,865	549,846	549,848	549,853	1.000502
27	549,776	549,778	549,764	549,773	549,773	1.000357
23	549,734	549,726	549,715	549,726	549,725	1.000269
19	549,704	549,695	549,685	549,701	549,696	1.000217
15	549,689	549,676	549,672	549,682	549,680	1.000187
11	549,677	549,660	549,663	549,678	549,670	1.000169
7	549,665	549,646	549,651	549,669	549,658	1.000147
3	549,648	549,631	549,637	549,656	549,643	1.000120
- 1	549,625	549,612	549,621	549,635	549,623	1.000084
- 5	549,605	549,595	549,601	549,610	549,605	1.000051
- 9	549,596	549,581	549,591	549,603	549,593	1.000029
-13	549,586	549,580	549,588	549,593	549,587	1.000018
-17	549,597	549,598	549,595	549,598	549,597	1.000036
-21	549,650	549,658	549,651	549,644	549,651	1.000135
-25	549,735	549,760	549,748	549,720	549,743	1.000302
-29	549,896	549,935	549,925	549,880	549,090	1.000604
-32	550,064	550,104	550,085	550,041	550,074	1.000904

APPENDIX A2

SOME QUANTITIES USED IN AVERAGING

$$b(z_1) = \frac{B_z(z_1) - B_z(z)}{B(\text{Monitor})}$$

Z	$\frac{B_z(z)}{B(\text{Monitor})}$	$\sqrt{b(35)}$	$\sqrt{b(31)}$	$\sqrt{b(27)}$	$\sqrt{b(19)}$	$\sqrt{b(7)}$
35	1.000743	0				
31	1.000502	.01552	0			
27	1.000356	.01967	.01208	0		
23	1.000270	.02175	.01523	.00927		
19	1.000216	.02296	.01691	.01183	0	
15	1.000185	.02362	.01780	.01308	.00557	
11	1.000168	.02398	.01828	.01371	.00693	
7	1.000146	.02443	.01887	.01449	.00837	0
3	1.000117	.02502	.01962	.01546	.00995	.00529
- 1	1.000084	.02567	.02045	.01649	.01149	.00787
- 5	1.000050	.02632	.02126	.01749	.01288	.00980
- 9	1.000026	.02678	.02182	.01817	.01378	.01095
-13	1.000019	.02691	.02198	.01836	.01404	.01127
-17	1.000042	.02648	.02145	.01772	.01319	.01020
-21	1.000134	.02468	.01918	.01490	.00906	.00346
-25	1.000302	.02100	.01414	.00738		
-29	1.000598	.01204				
-32	1.000888					
34*	1.000680	.00728				
33	1.000615	.01131				
30	1.000460		.00648			
29	1.000423		.00889			
26	1.000331			.00500		
25	1.000307			.00700		
18	1.000206				.00316	
17	1.000199				.00412	
6	1.000138					.00283
5	1.000132					.00374

*Values taken from graph of $B_z(z)$.

APPENDIX B1

DATA FOR 36 DIFFERENCE FREQUENCY RUNS

$C_2 = 40{,}000$

t	Run I X6 81 KV		Run III X3 114 KV		Run V X6 81 KV	
	C_1	C_1/C_2	C_1	C_1/C_2	C_1	C_1/C_2
1900	41,529	1.0398	40,686	1.0171	41,199	1.0299
1900.5	40,040	1.0009	40,927	1.0231	40,373	1.0092
1901	38,836	0.9708	39,838	0.9959	38,731	0.9682
1901.5	39,209	0.9802	38,504	0.9626	38,723	0.9681
1902	41,225	1.0305	41,037	1.0259	40,462	1.0114
1902.5	41,629	1.0409	41,228	1.0306	41,195	1.0298
1903	39,477	0.9869	39,559	0.9889	40,186	1.0046
1903.5	38,429	0.9607	38,642	0.9660	38,590	0.9647
1904	39,474	0.9868	40,343	1.0086	39,274	0.9818
1904.5	41,539	1.0384	41,623	1.0405	40,558	1.0139
1905	41,011	1.0253		.	41,080	1.0269
1905.5	39,403	0.9851				
300	38,936	0.9733	39,966	0.9992	39,021	0.9754
300.5	39,645	0.9911	38,169	0.9542	39,256	0.9813
301	40,893	1.0223	39,213	0.9803	40.220	1.0054
301.5	41,295	1.0324	41,464	1.0366	41,311	1.0327
302	39,763	0.9940	40,148	1.0037	40,212	1.0052
302.5	38,554	0.9638	37,853	0.9463	38,747	0.9686
303	39,898	0.9974	38,713	0.9678	38,968	0.9741
303.5	41.591	1.0397	40,783	1.0196	41,708	1.0427
304	40,647	1.0161	40,248	1.0062	41,693	1.0423
304.5	39,252	0.9813	38,131	0.9532	39.949	0.9987
305	38,455	0.9613			38,824	0.9705
305.5	40,310	1.0077			40,037	1.0009
f(Mon)	549,597 cps		649,638 cps		549,603 cps	

APPENDIX B1 (continued)

C_2 = 40,000

t	Run II X8 56 KV		Run IV X9 45 KV		Run VI X8 56 KV	
	C_1	C_1/C_2	C_1	C_1/C_2	C_1	C_1/C_2
1900	39,147	0.9786	40,158	1.0039	39,484	0.9871
1900.75	40,340	1.0084	39,913	0.9978	39,860	0.9964
1901.5	41,555	1.0388	39,096	0.9773	40,578	1.0144
1902.25	40,166	1.0040	39,623	0.9906	40,255	1.0064
1903	39,056	0.9763	40,679	1.0169	39,416	0.9854
1903.75	40,356	1.0089	39,921	0.9980	40,329	1.0082
1904.5	40,868	1.0216	39,756	0.9939	40,453	1.0113
1905.25	39,812	0.9952	39,343	0.9835	40,111	1.0027
1906	38,834	0.9708	40,766	1.0191	39,007	0.9751
1906.75	40,403	1.0100	40,358	1.0089	40,266	1.0066
1907.5			39,716	0.9929		
1908.25			39,286	0.9821		
1909						
300	39,718	0.9929	39,736	0.9933	39,779	0.9944
300.75	40,726	1.0181	39,756	0.9938	40,921	1.0230
301.5	39,725	0.9931	39,695	0.9923	40,139	1.0034
302.25	38,753	0.9687	40,573	1.0142	38,834	0.9708
303	39,860	0.9964	40,524	1.0130	39,473	0.9868
303.75	41,219	1.0305	39,538	0.9884	40,831	1.0208
304.5	39,866	0.9966	39,418	0.9854	40,077	1.0018
305.25	39,125	0.9780	40,295	1.0073	38,895	0.9724
306	39,703	0.9925	41,024	1.0255	39,993	0.9998
306.75	40,603	1.0150	40,042	1.0010		
307.5	39,894	0.9973	39,094	0.9975		
308.25	39,272	0.9817	39,936	0.9984		
f(Mon)	449,784 cps		399,780 cps		449,775 cps	

APPENDIX B1 (continued)

$C_2 = 40{,}000$

t	Run VII X3 114 KV		Run IX X6 81 KV		Run XI X3 114 KV	
	C_1	C_1/C_2	C_1	C_1/C_2	C_1	C_1/C_2
1900	42,207	1.0551	41,093	1.0273	40,328	1.0082
1900.5	41,009	1.0252	40,525	1.0131	41,136	1.0284
1901	38,290	0.9572	38,752	0.9688	39,992	0.9998
1901.5	39,329	0.9832	39,011	0.9753	38,595	0.9648
1902	41,482	1.0370	40,605	1.0151	40,418	1.0104
1902.5	40,928	1.0232	41,484	1.0370	41,390	1.0347
1903	38,675	0.9668	40,450	1.0112	39,974	0.993
1903.5	39,304	0.9826	38,690	0.9672	38,380	0.9594
1904			39,161	0.9789	40,431	1.0108
1904.5			40,771	1.0192	41,621	1.0405
1905			40,803	1.0201	39,854	0.9963
1905.5			39,524	0.9880		
300	39,184	0.9795	38,753	0.9688	40,152	1.0038
300.5	38,132	0.9532	38,844	0,9711	37,854	0.9463
301	40,718	1.0179	39,917	0.9978	39,185	0.9796
301.5	41,112	1.0280	40,982	1.0245	40,961	1.0240
302	38,721	0.9680	39,925	0.9981	40,517	1.0129
302.5	38,288	0.9571	38,439	0.9609	38,298	0.9574
303	40,104	1.0026	39,163	0.9790	38,754	0.9688
303.5	41,074	1.0268	40,832	1.0207	40,843	1.0211
304	39,420	0.9855	41,221	1.0305	40,319	1.0080
304.5			39,564	0.9891	38,277	0.9569
305					38,483	0.9620
f(Mon)	649,636 cps		549,593 cps		649,646 cps	

APPENDIX B1 (continued)

C_2 = 40,000

t	Run VIII X9 45 KV		Run X X8 56 KV		Run XII X9 45 KV	
	C_1	C_1/C_2	C_1	C_1/C_2	C_1	C_1/C_2
1900	40,011	1.0002	39,127	0.9781	40,466	1.0116
1900.75	40,076	1.0018	39,974	0.9993	39,739	0.9934
1901.5	39,845	0.9960	40,886	1.0221	39,904	0.9975
1902.25	39,947	0.9986	40,126	1.0031	39,587	0.9896
1903	40,664	1.0165	39,051	0.9762	40,561	1.0139
1903.75	40,351	1.0087	39,825	0.9956	40,013	1.0003
1904.5	39,575	0.9893	40,618	1.0154	39,902	0.9974
1905.25	39,402	0.9850	40,053	1.0013	39,506	0.9876
1906	40,370	1.0092	39,316	0.9829	40,491	1.0122
1906.75	40,645	1.0161	39,922	0.9980	40,490	1.0122
1907.5	40,019	1.0004			39,802	0.9950
1908.25	39,810	0.9952			39,604	0.9900
1909	40,203	1.0050			40,130	1.0032
300	40,021	1.0005	39,702	0.9925	49,570	1.0142
300.75	39,799	0.9949	40,811	1.0202	39,729	0.9934
301.5	39,879	0.9969	40,326	1.0082	39,620	0.9905
302.25	40,739	1.0184	39,299	0.9824	40,080	1.0020
303	40,331	1.0082	39,289	0.9822	40,864	1.0211
303.75	39,885	0.9971	40,740	1.0184	39,712	0.9927
304.5	39,776	0.9944	40,953	1.0013	39,703	0.9925
305.25	40,328	1.0082	39,290	0.9822	40,848	1.0211
306	40,660	1.0164	39,344	0.9836	40,713	1.0178
306.75	40.138	1.0034	49,941	1.0235	39,685	0.9921
307.5	39,798	0.9949	49,157	1.0039	39,493	0.9873
308.25	39,878	0.9968			39,501	0.9874
309					40,343	1.0085
f(Mon)	399,773 cps		449,769 cps		399,777 cps	

APPENDIX B1 (continued)

C_2 = 40,000

t	Run XIII X6 81 KV		Run XV X3 114 KV		Run XVII X6 81 KV	
	C_1	C_1/C_2	C_1	C_1/C_2	C_1	C_1/C_2
1900	41,601	1.0399	41,277	1.0319	41,214	1.0303
1900.5	41,044	1.0260	40,769	1.0192	41,286	1.0321
1901	39,521	0.9880	38,841	0.9709	39,852	0.9962
1901.5	38,443	0.9610	39,387	0.9847	38,518	0.9629
1902	39,671	0.9918	40,926	1.0231	39,609	0.9902
1902.5	41,143	1.0258	41,112	1.0278	41,080	1.0269
1903	41,156	1.0289	38,677	0.9669	41,325	1.0330
1903.5	39,050	0.9762	38,653	0.9663	39,399	0.9849
1904	38,756	0.9689	41,275	1.0318	38,470	0.9616
1904.5	40,431	1.0107	41,207	1.0301	40,019	1.0004
300	39,673	0.9918	38,783	0.9696	39,961	0.9990
300.5	38,720	0.9679	38,062	0.9515	38,388	0.9597
301	39,867	0.9967	39,481	0.9869	39,455	0.9863
301.5	41,673	1.0418	41,198	1.0299	41,581	1.0395
302	41,263	1.0315	39,163	0.9790	41,697	1.0424
302.5	38,933	0.9733	38,245	0.9561	39,734	0.9933
303	38,800	0.9699	40,273	1.0068	38,629	0.9657
303.5	40,725	1.0181	41,219	1.0305	49,393	1.0098
304	41,713	1.0428	39,275	0.9819	41,897	1.0474
304	41,713	1.0428	39,275	0.9819	41,897	1.0474
304.5	39,940	0.9984	38,201	0.9550	41,652	1.0412
f(Mon)	549,609 cps		649,642 cps		549,603 cps	

APPENDIX B1 (continued)

$C_2 = 40{,}000$

t	Run XIV X8 56 KV		Run XVI X9 45 KV		Run XIX X8 56 KV	
	C_1	C_1/C_2	C_1	C_1/C_2	C_1	C_1/C_2
1900	39,398	0.9849	40,320	1.0079	30,296	0.9823
1900.75	39,252	0.9813	40,220	1.0055	39,398	0.9849
1901.5	40,004	1.0001	39,926	0.9981	41,314	1.0328
1902.25	40,265	1.0065	39,610	0.9902	40,244	1.0060
1903	39,492	0.9872	40,315	1.0078	30,194	0.9798
1903.75	39,270	0.9817	39,973	0.9992	40,096	1.0024
1904.5	40,823	1.0205	39,740	0.9934	40,538	1.0134
1905.25	40,566	1.0141	39,412	0.9852	40,243	1.0060
1906	39,508	0.9877	39,894	0.9973	38,927	0.9731
1906.75	39,641	0.9909	40,384	1.0096	39,605	0.9901
1907.5	41,085	1.0271	40,015	1.0003	40,941	1.0235
1908.25	39,961	0.9989	39,219	0.9804	39,999	0.9999
1909	38,875	0.9718	39,673	0.9918		
300	39,153	0.9788	40,732	1.0182	39,478	0.9869
300.75	40,224	1.0056	39,796	0.9948	40,862	1.0215
301.5	40,722	1.0180	39,159	0.9789	40,328	1.0082
302.25	39,621	0.9905	40,416	1.0103	39,581	0.9894
303	39,722	0.9930	40,514	1.0128	39,084	0.9770
303.75	40,473	1.0118	39,998	0.9999	40,523	1.0130
304.5	40,486	1.0121	40,035	1.0008	40,461	1.0114
305.25	39,854	0.9962	39,908	0.9976	38,909	0.9726
306	39,601	0.9900	40,868	1.0217	39,825	0.9955
306.75	40,680	1.0170	40,214	1.0053	41,042	1.0260
307.5			39,678	0.9919	40,713	1.0178
308.25				39,615	0.9903	
309			40,388	1.0096		
f(Mon)	449,780 cps		399,767 cps		449,763 cps	

APPENDIX B1 (continued)

C_2 = 40,000

t	Run XVIII X3 114 KV		Run XXI X6 81 KV		Run XXII X3 114 KV	
	C_1	C_1/C_2	C_1	C_1/C_2	C_1	C_1/C_2
1900	38,724	0.9681	41,378	1.0344	39,010	0.9752
1900.5	41,707	1.0426	41,060	1.0265	41,463	1.0365
1901	40,735	1.0183	39,479	0.9869	41,026	1.0255
1901.5	38,483	0.9620	38,474	0.9618	38,874	0.9718
1902	39,127	0.9781	39,437	0.9859	38,949	0.9737
1902.5	41,394	1.0348	41,652	1.0413	41,320	1.0329
1903	40,612	1.0153	40,534	1.0133	41,070	1.0267
1903.5	38,757	0.9689	38,854	0.9713	38,818	0.9704
1904	38,495	0.9623	38,795	0.9698	38,890	0.9722
1904.5	31,391	1.0347	40,419	1.0105	41,281	1.0320
300	41,353	1.0338	39,180	0.9795	41,163	1.0290
[illegible].5	39,157	0.9789	38,696	0.9674	38,902	0.9725
301	38,504	0.9625	39,803	0.9950	38,379	0.9595
301.5	40,458	1.0114	41,443	1.0361	39,922	0.9980
302	41,023	1.0255	40,584	1.0145	41,275	1.0318
302.5	39,605	0.9901	39,223	0.9805	39,707	0.9926
303	37,693	0.9423	38,564	0.9640	38,161	0.9539
303.5	40,153	1.0037	40,767	1.0191	40,106	1.0026
304	41,602	1.0400	42,032	1.0508	41,227	1.0306
304.5	39,261	0.9815	40,544	1.0136	39,625	0.9906
f(Mon)	649,653 cps		549,604 cps		649,645 cps	

APPENDIX B1 (continued)

$C_2 = 40{,}000$

t	Run XX X9 45 KV		Run XXIII X8 56 KV		t	Run XXVII X8 56 KV	
	C_1	C_1/C_2	C_1	C_1/C_2		C_1	C_1/C_2
1900	40,445	1.0111	39,390	0.9847			
1900.75	40,254	1.0063	39,552	0.9887	1900	39,222	0.9804
1901.5	39,326	0.9830	40,660	1.0164	1900.75	39,548	0.9886
1902.25	39,481	0.9869	40,376	1.0094	1901.5	40,832	1.0207
1903	40,058	1.0014	38,484	0.9620	1902.25	40,809	1.0202
1903.75	40,317	1.0078	40,149	1.0037	1903	39,137	0.9784
1904.5	39,702	0.9925	40,886	1.0220	1903.75	39,549	0.9886
1905.25	39,786	0.9946	39,770	0.9941	1904.5	40,573	1.0142
1906	39,851	0.9961	39,195	0.9798	1905.25	40,684	1.0170
1906.75	40,765	1.0191	40,150	1.0037	1906	38,771	0.9692
1907.5	40,254	1.0063	41,035	1.0258	1906.75	39,127	0.9782
1908.25	39,964	0.9991	39,631	0.9907	300	39,017	0.9754
1909	39,843	0.9960			300.5	39,835	0.9959
300	40,573	1.0142	39,314	0.9828	301	40,850	1.0212
300.75	40,329	1.0081	40,869	1.0216	301.5	40,442	1.0110
301.5	39,827	0.9956	40,970	1.0242	302	39,861	0.9964
302.25	40,771	1.0192	39,456	0.9863	302.5	39,037	0.9758
303	40,845	1.0211	39,141	0.9784	303	39,050	0.9762
303.75	40,229	1.0057	40,683	1.0170	303.5	39,994	0.9998
304.5	39,851	0.9962	40,569	1.0142	304	40,353	1.0088
305.25	40,115	1.0028	39,261	0.9815	304.5	40,526	1.0131
306	40,797	1.0199	39,426	0.9856	305	39,945	0.9986
306.75	40,340	1.0084	40,627	1.0156	305.5	39,182	0.9794
307.5	39,883	0.9970			306	39,323	0.9831
308.25	39,932	0.9982			f(Mon)	449,787 cps	
309	40,281	1.0069					
f(Mon)	399,770 cps		449,768 cps				

APPENDIX B1 (continued)

$C_2 = 40{,}000$

t	Run XXIV X9 56 KV		Run XXXI X9 45 KV		t	Run XXVIII X9 45 KV	
	C_1	C_1/C_2	C_1	C_1/C_2		C_1	C_1/C_2
1900	40,594	1.0148	40,366	1.0091	1900	40,413	1.0103
1900.75	40,227	1.0056	39,837	0.9959	1900.75	40,453	1.0113
1901.5	39,792	0.9947	39,407	0.9851	1901.5	39,865	0.9965
1902.25	39,645	0.9911	39,461	0.9865	1902.25	39,868	0.9966
1903	40,405	1.0100	40,342	1.0085	1903	40,479	1.0119
1903.75	40,186	1.0046	40,346	1.0086	1903.75	40,588	1.0146
1904.5	39,804	0.9950	40,158	1.0039	1904.5	39,831	0.9957
1905.25	39,810	0.9952	39,401	0.9849	1905.25	39,437	0.9859
1906	40,000	1.0000	40,027	1.0006	1906	40,034	1.0008
1906.75	40,264	1.0065	40,374	1.0093	1906.75	40,495	1.0123
1907.5	39,940	0.9985	40,212	1.0053	1907.5	40,401	1.0100
1908.25	39,552	0.9887	39,822	0.9954	1908.25	39,585	0.9896
300	40,406	1.0100	40,760	1.0189	309	40,219	1.0054
300.75	39,612	0.9902	39,749	0.9937	309.75	40,393	1.0097
301.5	40,235	1.0058	39,989	0.9996	310.5	39,721	0.9929
302.25	40,499	1.0124	40,107	1.0026	311.25	39,411	0.9852
303	40,689	1.0172	40,678	1.0168	312	40,367	1.0091
303.75	40,436	1.0109	40,352	1.0088	312.75	40,683	1.0170
304.5	39,616	0.9903	39,829	0.9957	313.5	39,565	0.9891
305.25	40,267	1.0066	49,195	1.0048	314.25	39,113	0.9778
306	40,755	1.0188	40,368	1.0091	315	39,751	0.9938
306.75	40,058	1.0014	40,204	1.0050	315.75	40,517	1.0128
307.5	39,696	0.9923	39,943	0.9986	316.5	40,384	1.0096
308.25	39,563	0.9890	39,935	0.9983			
309	40,187	1.0046	40,489	1.0122	f(Mon)	399,772 cps	
f(Mon)	399,780 cps		399,775 cps				

APPENDIX B1 (continued)

$C_2 = 40{,}000$

t	Run XXV X6 81 KV		Run XXVI X3 114 KV		Run XXIX X3 114 KV	
	C_1	C_1/C_2	C_1	C_1/C_2	C_1	C_1/C_2
1900	40,825	1.0206	39,952	0.9987	39,295	0.9823
1900.5	40,282	1.0070	41,875	1.0468	41,505	1.0376
1901	38,853	0.9713	40,243	1.0060	40,708	1.0177
1901.5	39,040	0.9760	38,227	0.9556	38,646	0.9661
1902	40,412	1.0103	39,717	0.9929	39,217	0.9804
1902.5	41,811	1.0452	41,279	1.0319	41,268	1.0317
1903	40,178	1.0044	40,226	1.0056	41,342	1.0335
1903.5	38,328	0.9582	38,195	0.9548	38,527	0.9632
1904	39,226	0.9806	39,785	0.9946	39,246	0.9811
1904.5	40,599	1.0149	41,265	1.0316	41,571	1.0392
1905	41,473	1.0368				
300	38,906	0.9726	40,738	1.0184	41,110	1.0277
300.5	39,454	0.9863	38,572	0.9643	38,702	0.9675
301	40,750	1.0187	38,034	0.9508	38,164	0.9540
301.5	41,559	1.0390	40,331	1.0082	40,551	1.0137
302	40,016	1.0004	40,921	1.0230	41,811	1.0452
302.5	38,506	0.9626	38,612	0.9652	38,815	0.9704
303	39,372	0.9842	38,561	0.9640	37,740	0.9434
303.5	41,358	1.0338	40,552	1.0138	40,316	1.0079
304	41,676	1.0418	41,105	1.0276	41,390	1.0347
304.5	40,110	1.0027	38,882	0.9720	38,656	0.9664
305					38,441	0.9610
f(Mon)	549,610 cps		649,646 cps		649,645 cps	

APPENDIX B1 (continued)

$C_2 = 40{,}000$

t	Run XXX X6 81 KV		Run XXXV X3 114 KV		Run XXXIII X6 81 KV	
	C_1	C_1/C_2	C_1	C_1/C_2	C_1	C_1/C_2
1900	41,430	1.0357	39,032	0.9758	40,269	1.0067
1900.5	40,911	1.0227	40,850	1.0212	41,903	1.0475
1901	39,000	0.9749	41,433	1.0358	40,233	1.0058
1901.5	38,598	0.9649	38,928	0.9732	38,334	0.9583
1902	39,871	0.9968	38,388	0.9597	39,182	0.9795
1902.5	41,290	1.0322	40,486	1.0121	40,829	1.0206
1903	41,172	1.0292	41,649	1.0412	41,306	1.0326
1903.5	38,657	0.9664	39,070	0.9767	39,795	0.9948
1904	38,599	0.9649	38,284	0.9570	38,490	0.9622
1904.5	40,709	1.0176	40,842	1.0210	39,716	0.9928
1905			41,940	1.0485	41,140	1.0285
300	38,878	0.9719	41,444	1.0361	40,295	1.0073
300.5	39,165	0.9790	39,779	0.9944	38,865	0.9715
301	40,126	1.0031	38,213	0.9553	39,845	0.9960
301.5	42,006	1.0500	39,693	0.9923	40,884	1.0220
302	40,859	1.0214	41,431	1.0358	41,689	1.0422
302.5	39,255	0.9813	40,263	1.0065	39,836	0.9958
303	38,784	0.9695	38,268	0.9567	38,467	0.9616
303.5	40,738	1.0184	39,506	0.9876	39,471	0.9867
304	41,670	1.0417	41,425	1.0356	41,505	1.0375
304.5	40,399	1.0098	40,474	1.0118	41,202	1.0300
305					39,071	0.9767
305.5	549,604 cps		649,637 cps		549,606 cps	

APPENDIX B1 (continued)

C_2 = 40,000

t	Run XXXII X8 56 KV		Run XXXVI X8 56 KV		t	Run XXXIV X9 45 KV	
	C_1	C_1/C_2	C_1	C_1/C_2		C_1	C_1/C_2
1900	39,701	0.9925	39,844	0.9960	1906.75	40,457	1.0114
1900.75	39,742	0.9934	38,933	0.9732	1907.5	40,570	1.0142
1901.5	40,561	1.0140	40,285	1.0071	1908.25	39,527	0.9881
1902.25	40,515	1.0128	40,506	1.0126	1909	39,880	0.9969
1903	39,841	0.9959	40,039	1.0009	1909.75	40,003	1.0000
1903.75	39,938	0.9938	38,805	0.9701	1910.25	40,840	1.0209
1904.5	40,920	1.0229	40,429	1.0107	1911	40,682	1.0170
1905.25	40,722	1.0180	40,896	1.0223	1911.75	39,293	0.9823
1906	39,395	0.9848	39,968	0.9992	1912.5	40,207	1.0051
1906.75	39,345	0.9836	39,286	0.9821	1913.25	40,005	1.0000
1907.5			40,220	1.0054	1914	40,381	1.0095
1908.25			40,810	1.0201	1914.75	40,100	1.0024
300	39,125	0.9781	39,096	0.9774	308.25	39,434	0.9858
300.75	40,426	1.0106	39,743	0.9935	309	39,860	0.9964
301.5	40,944	1.0236	40,755	1.0188	309.75	40,066	1.0016
302.25	39,721	0.9930	39,933	0.9983	310.5	397,48	0.9937
303	39,365	0.9841	39,494	0.9873	311.25	39,300	0.9824
303.75	40,488	1.0122	39,792	0.9947	312	39,889	0.9971
304.5	41,185	1.0295	40,401	1.0099	312.75	40,417	1.0104
305.25	39,645	0.9911	40,016	1.0003	313.5	40,221	1.0054
306	39,470	0.9867	39,595	0.9898	314.25	39,229	0.9807
306.75	40,384	1.0095	40,053	1.0013	315	39,395	0.9848
307.5	40,755	1.0188	40,672	1.0168	315.75	40,195	1.0048
308.25			39,970	0.9992	316.5	40,322	1.0080
309					317.25	39,781	0.9944
f(Mon)	449,775 cps		449,774 cps		f(Mon)	399,767 cps	

APPENDIX B2

COMPUTED MAXIMA AND AVERAGES

X6 RUNS

Run	Hi Max	Lo Max	N	τ_D	$\tau_D f$(Mon)	Weight
I	1904.700	301.275	672	2.38605	1.311366	4.18
V	1904.825	301.425	672	2.38601	1.311358	3.53
IX	1902.450	301.450	671	2.38599	1.311323	2.26
XIII	1902.650	301.600	671	2.38607	1.311406	3.37
XVII	1902.725	301.750	671	2.38595	1.311325	5.52
XXI	1902.675	301.600	671	2.38610	1.311410	3.55
XXV	1902.450	301.400	671	2.38607	1.311408	2.99
XXX	1902.575	301.550	671	2.38603	1.311372	3.34
XXXIII	1902.850	301.825	671	2.38603	1.311376	3.61

Weighted Average = 1.311370

X8 RUNS

Run	Hi Max	Lo Max	N	τ_D	$\tau_D f$(Mon)	Weight
II	1904.400	300.850	550	2.91554	1.311363	2.41
VI	1904.475	300.900	550	2.91559	1.311359	2.32
X	1904.525	301.050	550	2.91541	1.311261	2.53
XIV	1904.800	301.275	550	2.91550	1.311334	1.75
XIX	1904.600	301.125	550	2.91541	1.311243	1.89
XXIII	1907.425	301.200	551	2.91511	1.311123	1.87
XXVII	1904.750	301.275	550	2.91541	1.311313	2.58
XXXII	1904.825	301.375	550	2.91536	1.311256	2.27
XXXVI	1905.100	301.625	550	2.91541	1.311276	2.06

Weighted Average = 1.311301

APPENDIX B2 (continued)

X3 RUNS

Run	Hi Max	Lo Max	N	τ_D	τ_D f(Mon)	Weight
III	1902.375	30.1600	793	2.01863	1.311379	3.27
VII	1902.150	301.350	793	2.01866	1.311394	4.07
XI	1904.475	301.650	794	2.01867	1.311421	4.31
XV	1904.250	301.400	794	2.01870	1.311432	3.37
XVIII	1902.700	301.900	793	2.01866	1.311428	3.64
XXII	1900.700	301.925	792	2.01866	1.311412	5.65
XXVI	1902.550	301.800	793	2.01860	1.311375	4.50
XXIX	1902.675	301.850	793	2.01869	1.311432	4.24
XXXV	1904.850	302.075	794	2.01861	1.311364	4.27

Weighted Average = 1.311404

X9 RUNS

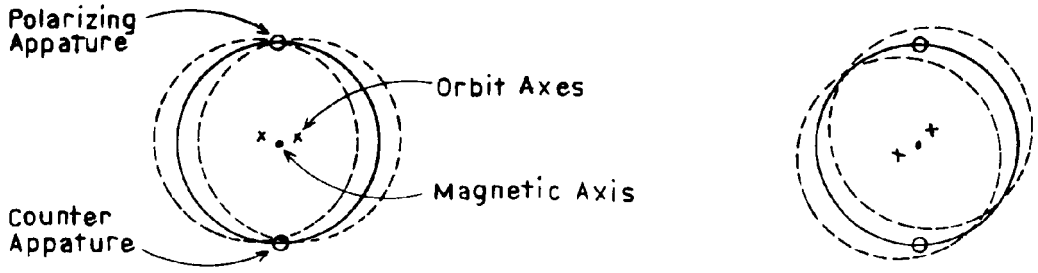
Run	Hi Max	Lo Max	N	τ_D	τ_D f(Mon)	Weight
IV	1906.425	302.575	489	3.27986	1.311222	1.27
VIII	1906.525	302.575	489	3.28006	1.311279	1.31
XII	1906.450	302.700	489	3.27965	1.311129	1.05
XVI	1906.775	302.925	489	3.27986	1.311180	1.39
XX	1903.550	302.900	488	3.28002	1.311254	1.17
XXIV	1903.400	302.800	488	3.27992	1.311246	1.12
XXVIII	1906.850	312.625	486	3.28030	1.311372	1.78
XXXI	1906.800	302.925	489	3.27991	1.311226	1.15
XXXIV	1910.425	309.650	488	3.28028	1.311348	1.16

Weighted Average = 1.311252

APPENDIX C1

ORBITAL PRECESSION AND THE FALLOFF INDEX

A graph of Counting Rate vs. Trapping Time is shown in Figure 16. The rather strong periodic dependence of counting rate on trapping time for times below 200 microseconds occurs because the axes of the orbits of most electrons in the beam do not coincide exactly with the magnetic axis. This is due to the finite size of the solid angle accepted from the polarizing target. Figure 15 shows the end view of a beam which has been peaked up at zero trapping time. The counting rate is maximum



Trapping Time = 0 (a)

Trapping Time = t (b)

Beam Cross Section

Figure 15.

in 15(a) because the orbits converge at the radius of the counter apperture.

In nearly homogeneous magnetic fields

$$B_z = Kr^n \quad , \quad n \ll 1 \ . \tag{C1}$$

Then it is easily shown that the orbit axes describe a circle around the magnetic axis with frequency

$$\Omega = \frac{1}{2} n\omega_c \ , \tag{C2}$$

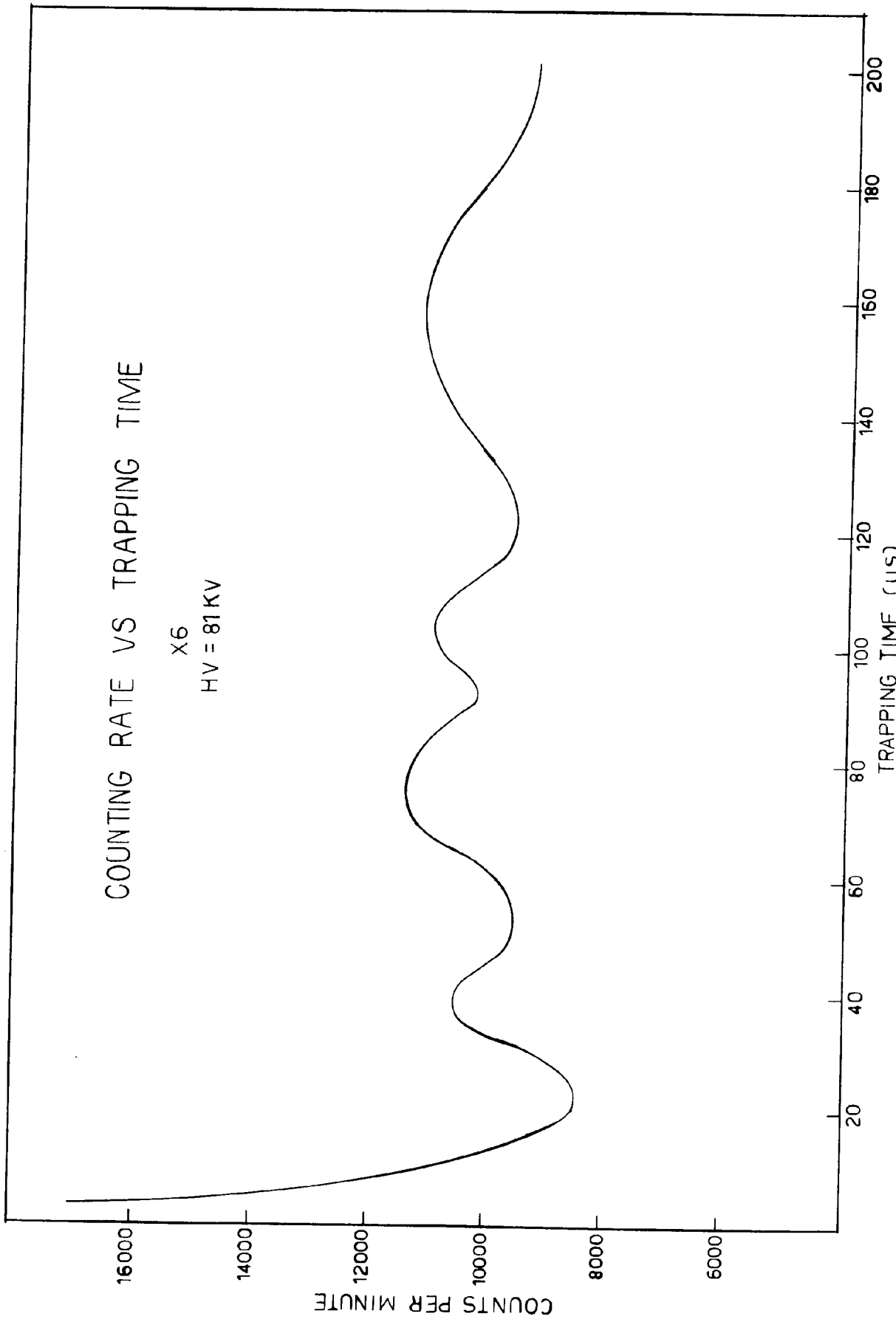

COUNTING RATE VS TRAPPING TIME
X6
HV = 81 KV
COUNTS PER MINUTE
16000
14000
12000
10000
8000
6000
20
40
60
80
100
120
140
160
180
200
TRAPPING TIME (μs)

Figure 16

where ω_c is the cyclotron frequency and n is the falloff index of the magnetic field. Note that

$$n = \frac{r}{B_z}\frac{\partial B_z}{\partial r} \quad . \tag{C3}$$

Therefore, at some trapping time t the beam cross section looks like Figure 15(b) and only a fraction of the beam (those particles with orbital axes very near the magnetic axis) can be scattered into the counter aperture. Since in a bottle-shaped (trapping) field $n < 0$, the orbital precession Ω has a direction opposite to the direction of ω_c.

From the above arguments one would expect two peaks to occur during one cycle of the orbital precession. Therefore, we may evaluate Ω from the curve in Figure 16:

$$\Omega = -\frac{2\pi}{2T} = -8.3 \times 10^4 \text{ rad./sec} \quad , \tag{C4}$$

where T is the time between adjacent peaks. The cyclotron frequency for the energy used to obtain Figure 16 is

$$\omega_c = \frac{\beta c}{R} = 2.0 \times 10^9 \text{ rad./sec} \quad . \tag{C5}$$

Thus, from (C2)

$$n = -8.3 \times 10^{-5} \quad , \tag{C6}$$

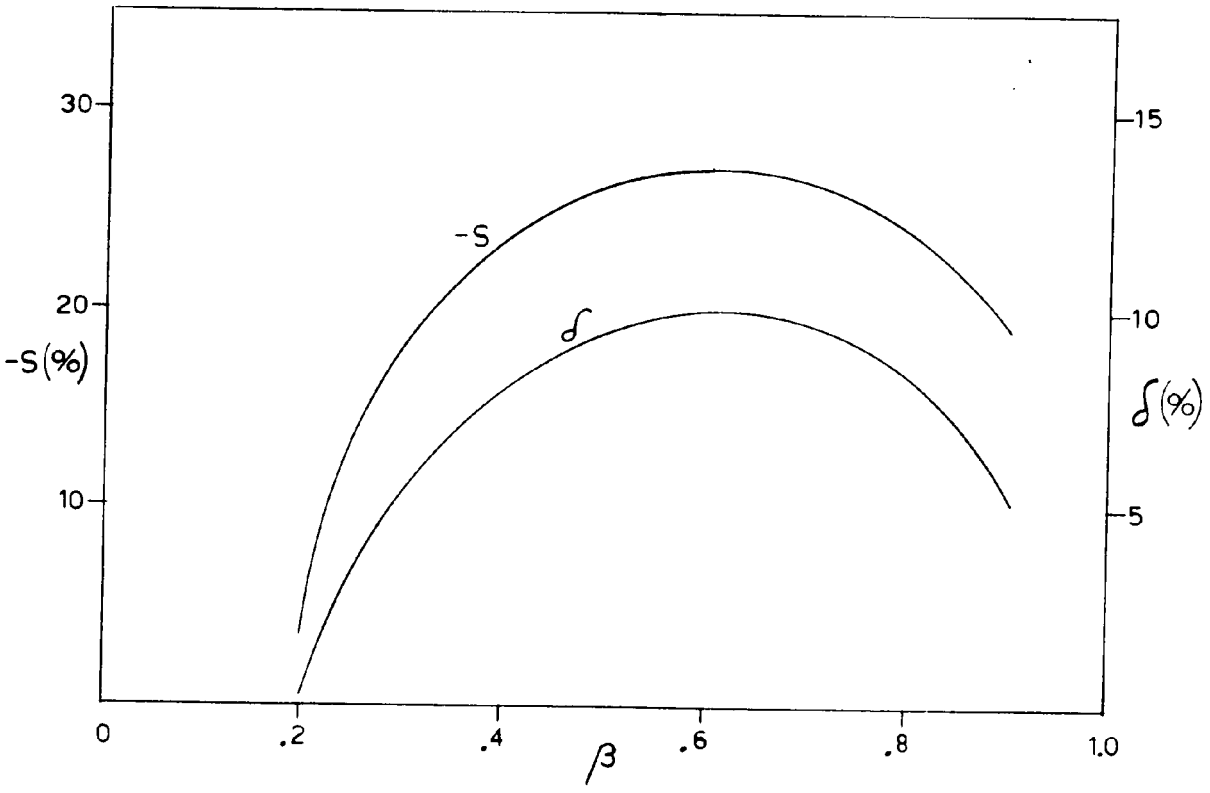
for the magnetic well used in this experiment. This value agrees with estimates of n from the magnetic field map.

APPENDIX C2

THEORETICAL POLARIZATION AND ASYMMETRY AMPLITUDE

The percent polarization (S) and asymmetry amplitude (δ) as calculated by Sherman [22] are tabulated and plotted as functions of β. The parameters used are, $\theta_1 = 90^\circ$, $\theta_2 = 105^\circ$, $\phi_2 = 0^\circ$, $Z = 80$.

β	T(KV)	-S(%)	δ(%)
.2	10.5	3.6	.73
.4	45	23.4	7.79
.5	79	26.1	9.29
.6	127	27.1	9.95
.7	204	26.5	9.65
.8	340	24.2	8.23
.9	662	19.0	5.26



APPENDIX C3

VERIFICATION OF EQUATION (4.3) FOR THE MAGNETIC FIELD IN THE TRAPPING REGION

The field of a solenoid of radius R, length L, and N turns/cm carrying I abampheres, can be expressed in a power series of the radius r:

$$B_z(r,z) = \sum_{n=0}^{\infty} \frac{(-1)^n}{(n!)^2} B_z^{(2n)}(0,z) \left(\frac{r}{2}\right)^{2n} , \qquad (C7)$$

$$B_r(r,z) = \sum_{n=0}^{\infty} \frac{(-1)^{n+1}}{(n!)^2 (n+1)} B_z^{(2n+1)}(0,z) \left(\frac{r}{2}\right)^{(2n+1)} , \qquad (C8)$$

where $B_z^{(n)}$ is the n^{th} derivative of the field on the axis:

$$B_z(0,z) = 2\pi NI \left[\frac{z+L}{\sqrt{(z+L)^2 + R^2}} - \frac{z-L}{\sqrt{(z-L)^2 + R^2}} \right] . \qquad (C9)$$

The corrected solenoid used in this experiment can be thought of as the superposition of two coaxial solenoids. A main solenoid of 10 layers carrying current +I and a shorter correction solenoid of 2 layers carrying -I. The correction solenoid has the same center and radius as the outer 2 layers of the main solenoid and, therefore, cancels the effect of these layers except at the ends. The result is an 8-layer solenoid with 2-layer correcting solenoids at each end, carrying the same current, +I. Therefore, the field in the trapping region can be represented analytically by the difference of two power series, one for the 10-layer solenoid and one for the two layer solenoid:

$$B_z = \sum \frac{(-1)^n}{(n!)^2} \Delta B_z^{(2n)}(0,z) \left(\frac{r}{2}\right)^{2n} , \qquad (C10)$$

and

$$B_r = \sum \frac{(-1)^{n+1}}{(n!)^2 (n+1)} \Delta B_z^{(2n+1)}(0,z) \left(\frac{r}{2}\right)^{(2n+1)} , \qquad (C11)$$

where

$$\Delta B_z^{(m)}(0,z) = B_z^{(m)}(0,z)_{10\text{-layer}} - B_z^{(m)}(0,z)_{2\text{-layer}} , \qquad (C12)$$

represents the m^{th} derivative of the resultant field on the axis.

We wish to express the following integral in terms of the measured quantity $B_z(z)$:

$$\frac{1}{2} m v_z^2 = \frac{e v_\theta}{c} \int_{z_1}^{z} B_r dz , \qquad (4.2)$$

where z_1 is an arbitrarily chosen amplitude near the end of the trapping region, and z is inside the trapping region. Consider the following quantities:

$$-\frac{2}{r} \int_{z_1}^{z} B_r dz = \sum_{n=0}^{\infty} \frac{(-1)^n}{(n!)^2 (n+1)} \left[\Delta B_z^{(2n)}(0,z) - \Delta B_z^{(2n)}(0,z_1)\right] \left(\frac{r}{2}\right)^{2n} , \qquad (C13)$$

and

$$B_z(z) - B_z(z_1) = \sum_{n=0}^{\infty} \frac{(-1)^n}{(n!)^2} \left[\Delta B_z^{(2n)}(0,z) - \Delta B_z^{(2n)}(0,z_1)\right] \left(\frac{r}{2}\right)^{2n} . \qquad (C14)$$

The power series expansions are the same except for a factor of $(n + 1)^{-1}$ in (C13). Therefore, the first terms ($n = 0$) are identical, the second terms differ by a factor of 2, etc. The first two terms have been evaluated numerically for the solenoid used in this experiment. It was found that, for points on the beam radius and separated by 5 cm, the values of (C13) and (C14) differ by less than 5%. Therefore, for the purposes of Section 4.1 the following approximation is sufficient:

$$\int_{z_1}^{z} B_r dz = -\frac{R}{2}\left[B_z(z) - B_z(z_1)\right] \quad , \qquad (C15)$$

where R is the beam radius and is dropped from the argument of B_z. Equation (C15) also follows directly from Maxwell's Equations if one assumes (1) cylindrical symmetry and (2) that the second derivatives of B_r with respect to r and z are much smaller than B_r/R^2 in the trapping region. However, assumption (2) is difficult to verify.

APPENDIX C4

LIST OF EXPERIMENTAL PARAMETERS

Settings for Final Data

	X3	X6	X8	X9
Crystal Frequency	650.12 kc	550.01 kc	450.12 kc	400.08 kc
Magnetic Field	153 gauss	129 gauss	106 gauss	94 gauss
Electron Energy	114 KV	81 KV	56 KV	45 KV
Max. Well Depth	-55 ev	-40 ev	-27 ev	-22 ev
Ejection Voltage	18 volts	26 volts	23 volts	15 volts
Min. Well Amplitude	29 cm	27 cm	21 cm	23 cm
Avg. Period in Well	0.38 μs	0.44 μs	0.53 μs	0.60 μs

Other Parameters

Beam Radius = 7.6 cm

Vacuum in Trapping Region = 2×10^{-7} mm of Hg.

Trapping time = 300 to 1900 microseconds.

Beam Pulse Length = 0.2 microseconds.

Number of Electrons in Trap = 10^5 to 10^6.

Injection Pulse Voltage = 50 volts.

Counting Rate = 5,000 to 10,000 CPM.

Repetition Rate = 500 cps.

Timing Clock Frequency = 999,982 cps.

Thickness of Gold Targets = 10^{-5} cm.

LIST OF REFERENCES

1. P. A. M. Dirac, Proc. Roy. Soc. (London) A117, 610 (1927); A118, 351 (1928).
2. G. E. Uhlenbeck and S. Goudsmit, Nature 117, 264 (1926).
3. W. E. Lamb, Jr. and R. C. Retherford, Phys. Rev. 72, 241 (1947).
4. H. A. Bethe, Phys. Rev. 72, 339 (1947).
5. J. Schwinger, Phys. Rev. 73, 416 (1948); 74, 1439 (1948); 75, 651 (1949); 76, 790 (1949).
6. R. Karplus and N. M. Kroll, Phys. Rev. 77, 536 (1950).
7. C. M. Sommerfield, Phys. Rev. 107, 328 (1957), Ann. Phys. 5, 26 (1958).
8. A. Petermann, Nucl. Phys. 5, 677 (1958); P. Smarz and I. Ulehla, Czech. J. Phys. 10, 966 (1960).
9. P. Kusch and H. M. Foley, Phys. Rev. 74, 250 (1948).
10. P. Franken and S. Liebes, Jr., Phys. Rev. 104, 1197 (1956).
11. W. A. Hardy and E. M. Purcell, Private Communication, 1958.
12. S. H. Koenig, A. G. Prodell, and P. Kusch, Phys. Rev. 88, 191 (1952).
13. R. Beringer and M. A. Heald, Phys. Rev. 95, 1474 (1954).
14. J. S. Geiger, V. W. Hughes, and H. E. Radford, Phys. Rev. 105, 183 (1957).
15. J. W. M. Dumond, IRE Trans. on Instrumental 1-7, 136 (1958).
16. H. R. Crane, R. W. Pidd, and W. H. Louisell, Phys. Rev. 94, 7 (1954).
17. See for example: Mott and Massey, The Theory of Atomic Collisions, Oxford University Press, London (1959), p. 63.
18. H. Mendlowitz and K. M. Case, Phys. Rev. 97, 33 (1955).
19. H. R. Crane, R. W. Pidd, and A. A. Schupp, Phys. Rev. 121, 1 (1961).
20. W. E. Lamb, Jr., Phys. Rev. 85, 259 (1952).
21. S. Triebwasser, E. S. Dayhoff, and W. E. Lamb, Jr., Phys. Rev. 89, 98 (1953).
22. N. Sherman, Phys. Rev. 103, 1601 (1956).

23. F. Mandl, Introduction to Quantum Field Theory, Interscience, New York (1959), p. 148.

24. W. Heitler, The Quantum Theory of Radiation, Third Edition, Oxford University Press, London (1954), p. 311.

25. G. W. Ford and C. W. Hirt, University of Michigan, 1961, (unpublished).

26. L. H. Thomas, Phil. Mag. 3, 1 (1926). Corben and Stehle, Classical Mechanics Wiley, New York (1950), p. 355.

27. G. W. Ford, Private Communication, 1962.

28. R. V. Pound and W. D. Knight, Rev. Sci, Instr. 21, 219 (1950).

29. R. J. Blume, Rev. Sci. Instr. 29, 574 (1958).

30. D. F. Nelson and R. W. Pidd, Phys. Rev. 114, 728 (1959).

31. N. Ryu, J. Phys. Soc. Japan 5, 423 (1950).

32. M. E. Rose and H. A. Bethe, Phys. Rev. 55, 277 (1939).

33. J. M. W. DuMond, Ann. of Phys. 7, 365 (1959).